Design and fabrication of glucose sensor using metal-organic framework nanomaterials

Yazdan Firouzi Jahantigh, Mehdi Mehrpooya, Reza Askari Moghadam, Mohammad Reza Ganjali

Design and fabrication of glucose sensor using metal-organic framework nanomaterials

Yazdan Firouzi jahantigh[1], Mehdi Mehrpooya [2*], Reza Askari Moghadam[3], Mohammad Reza Ganjali[4]

[1] College of Interdisciplinary Science and Technology, University of Tehran, Tehran, Iran

[1]School of Energy Engineering and Sustainable Resources, College of Interdisciplinary Science and Technology, University of Tehran, Tehran, Iran

[3]Sorbonne Université, CNRS, INSERM, Laboratoire d'Imagerie Biomédicale, LIB, F-75006, Paris, France

[3]Center of Excellence in Electrochemistry, School of Chemistry, College of Science, University of Tehran, P.O. Box 11155-4563, Tehran, Iran

****

A MEMS systems integrate mechanical components, sensors, actuators, and electronics on the same silicon substrate using microfabrication technology. Micromechanical parts are made by micromachining processes that selectively etch part of the silicon substrate or deposit layers of a new structure. In this work, these structures and their building blocks are presented, and a nano-network of metal-organic compounds is reported for the synthesis and recognition of glucose. The morphological structure of the prepared sample was observed through scanning electron microscopy. At the same time, the structure and characteristics of the metal-organic framework crystals were examined using scanning electron microscopy mapping and analysis tests like energy-dispersive X-ray spectroscopy, X-ray diffraction analysis, Raman spectroscopy, and

[*] Corresponding author. School of Energy Engineering and Sustainable Resources, College of Interdisciplinary Science and Technology, University of Tehran, Tehran, Iran. E-mail addresses: mehrpoya@ut.ac.ir (M. Mehrpooya).

infrared spectroscopy. This prepared material was inserted into a microstructure and evaluated as a glucose sensor. This all leads to the final microstructure that arises from the integration of the microscale technology with the electrochemical sensing systems. Both the electrochemical structure and the microscale chip are integrated to achieve the final structure, which includes microchannels and a three-electrode system comprising a reference electrode, a counter electrode, and a working electrode for the reaction and detection of glucose levels. Finally, the microscale chip, made from polycarbonate sheets, is placed on the three-electrode system, secured, and the design and construction of this microscale sensor enable the measurement of various glucose concentrations. Glucose sensing was performed using cyclic voltammetry and chronoamperometry processes by directing glucose-containing fluid through the structural channels toward the electrodes. The best electrocatalytic behavior towards glucose oxidation in 0.1 molar potassium hydroxide environments was attained. During these processes, a high sensitivity of 35,000 microamperes per millimolar square centimeter in the linear range of 0 to 6 micromolar with a very low detection limit of 0.18 micromolar and a correlation coefficient of 0.998 (R^2) was obtained.

Keywords: Metal-organic framework, synthesis, glucose sensor, microstructures, electrocatalyst, cyclicvoltammetry,chronoamperometrybstract

Highlights

- Incorporation of lanthanides and ZIF-8 shows acceptable performance for cyclic voltammetry (CV) and chronoamperometry

- The impact of using lanthanum metal on electrochemical aspects has been investigated.

- In this study, a printed three-electrode system made of gold was used for the analysis of a microfluidic sensor.

Nomenclature

ZIF	Zeolitic Imidazole Framework		
MOF	Metal Organic Framework	Zn	Zincc
MEMS	Microelectromechanical	K	Potassium
CV	Cyclic Voltammetry	H	Hydrogen
AUE	Gold Electrodes	Ag	Silver
NPC	N-Doped Porous Carbons	AR	Argon
XRD	X-Ray Diffraction	La	Lanthanum
SEM	Scanning Electron Microscopy	DMF	Dimethyl Form amide
		KOH	Potassium Hydroxide
FTIR	Fourier Transformed Infrared	*Parameters of the electrochemical measurements*	
EDS	Energy-Dispersive X-ray Spectroscopy	J	Current density (mA cm^{-2})
TEM	Transmission Electron Microscopy	Δt	Discharge time (s)
		mM	Mille Molar(concentration)
Elements		Δv	Voltage window (V)
C	Carbon	ΔI	Current window
N	Nitrogen		
O	Oxygen		
H	Hydrogen		

1. Introduction

Glucose detection is one of the major significant areas in clinical, pharmaceutical, chemical, biological, fermentation, and bioenergy industries. In clinical medicine, diabetes or sweet sugar is regarded as one of the factors contributing to the burden of disabilities and death across the globe. It is a metabolic disease emanating from the inefficiency of insulin that allows blood glucose concentration to increase beyond its normal range. Clinical quantification of blood glucose is thus very important; this would prevent most of the incidents of heart disease, renal failures, and blindness caused by diabetes. Diabetes is a chronic disease caused by defects in insulin secretion or function. According to the World Health Organization, the number of people afflicted with diabetes worldwide may rise to as many as 400 million by the year 2025. Clinical Presentation: In most cases, clinically presented patients with diabetes are suffering from persistent hyperglycemia and may also suffer from further complications including kidney failure, blindness, and cardiovascular diseases. Accurate diagnosis and evaluation of blood glucose concentration are important for individual diagnosis and evaluation. Besides, it is very important for blood glucose level monitoring at frequent and long time intervals for maintaining it within the normal range and preventing its further complication. Skin-based diagnosis among all the detection techniques provides the most efficient approach for glucose detection [1]Although many types of biosensors of different principles have been developed so far, each having possible application value, none can achieve simultaneously non-invasive, micro/nano

scales of continuity, high sensitivity, and low detection limits. Thus, many challenges remain unanswered from diabetes monitoring technology so far, offering a wide avenue for research. The basis of the two principles of measurement of blood glucose in different devices is photometric and electrochemical. This photometric technique thus relies on an internal light source to make an approximation of the glucose level inside the blood. Through an enzymatic reaction, glucose gets converted into some colored compound. Light, inside the device at a particular wavelength, falls on the blood glucose test strip where the colored compound, being pre-generated, gets absorbed. The amount of colored compound generated is directly proportional to the glucose level of the concerned individual. The higher the glucose level, the more color produced, which the strip absorbs more light accordingly[2]. Thus, it reflects less light hence giving the level of the blood glucose to the doctor or the person. In the electrochemical technique, glucose is enzymatically oxidized and produces electrons. The amount of electrons trapped depends upon the glucose level present in the sample[3][4].The higher the glucose level, the higher the percentage of electrons produced. On the other hand, at a low level of glucose, the percentage produced will equally be low. Moreover, the device should be very clean to function well. This is very important in the photometric method. However, a number of the patients do not know, and even these few who know, give little attention to cleaning the device. Therefore, for an accurate reading, the glass surface should be cleaned well to give a perfect reflection of light. The electrochemical technique does not apply the principle of light, hence it is not badly affected by dirtiness in the setting[5]. Wrist wear blood glucose monitor, by the name appears like a watch. It is worn on the wrist, where one can measure the glucose in the blood with no pain and bleeding. This would involve a small, fine needle used to

prick the finger lightly in order to get an adequate amount of blood to measure the level of glucose. A blood sample is then placed onto a special test strip in the device, which would then measure the glucose. Such a device is highly recommended for being present in every house of people suffering from diabetes[6][7].In this respect, the non-enzyme sensors could be considered as one of the valid alternatives to the fourth generation[8]. A new and exciting class of porous hybrid materials, MOFs form by the self-assembly of metal ions or clusters with organic ligands. Materials that are defined as nanomaterials have at least one dimension within the nanometer range (1-100 nm) or a component or phase within the nanometer scale[9]. Since their discovery, MOFs have drawn wide attention due to their unprecedented structure and characteristics. Nanoparticles, due to their nano-size, possess unique properties as compared to their bulky homologues. For instance, Nano catalysts provide a greater surface area, hence more availability of catalytic sites.[10] Besides, the shorter diffusing distances in nanocrystals favor the contact of substrate with catalytic center and hence allow a higher catalytic activity compared to the related bulk materials[11]. Nanomaterials also display novel optical, electrical, magnetic, and thermal characteristics due to quantum effects and other phenomena associated with their small size. These materials are widely used across fields such as Nano electronics, medicine and healthcare, aerospace, environmental science, energy storage, and biotechnology[12].MOFs, in particular, stand out for their high surface area, structural versatility, and flexibility. These characteristics make them useful in a range of applications, including catalysis[13], gas storage and separation[14][15], biomedical fields[16][17], chemical sensing[18][19], and energy storage and conversion, among others Recently, there has been a growing interest in nano-sized MOFs (nanoMOFs), which have at least one dimension in the nanometer range. Accordingly,

nanoMOFs have distinct advantages: faster adsorption/desorption kinetics, better accessibility of the interior active sites for catalysis, adequate sizes for biomedical applications, and the possibility of various nanostructures enhancing the performance either in energy applications or in membrane separations. In this paper, the structure of MOFs will be introduced, as well as discussion of a number of synthesis methods[20][21].MOFs are structurally composed of two major components: secondary building units-clusters or metal ions-and organic linkers. In principle, any number of MOF structures can be created by combining these elements in various ways. Furthermore, within each framework geometry, it is possible to substitute the metal center, and that further provides even larger diversity. For instance, changing secondary building units with one organic linker-common terephthalic acid-can yield completely different MOFs. This wide range of building blocks and connectivity options has led to the creation of a large number of MOF structures[15]. Notably, since the groundbreaking work of Furukawa and colleagues, over 20,000 types of MOFs have been reported and studied within the past decade. Among other advanced Nano catalysts, there are 3D carbon aerogels derived from biomass, which contain dual-metal nanoparticles encapsulated within a carbon shell in carbon nanotubes (CNTs). These unique structures increase the active surface area and improve electron transfer, making them highly effective for microfluidic fuel cells. Their robust 3D design also makes them durable, particularly for applications like ethylene glycol fuel cells[22].This catalyst features trimetallic Ni–Cu nanoparticles arranged in a rhombic dodecahedron shape and is loaded onto flexible butter sheet paper. It offers excellent electrical conductivity and numerous active sites for glucose oxidation, making it a highly sensitive and efficient non enzymatic glucose sensor[23].Cobalt oxide nanoparticles in this structure form interconnected needle-like shapes,

which provide a large active surface area, low resistance to charge transfer, and excellent stability. This catalyst is particularly well-suited for non enzymatic glucose sensors due to its high sensitivity, low detection limit, and long-term stability against degradation.[24]This combination of graphene, CNTs, and nickel serves as a polysulfide trap, preventing the loss of polysulfide's and increasing the lifespan and capacity of lithium-sulfur batteries[25]Ni-Co bimetallic nanowires embedded within CNTs are designed for nonenzymatic glucose sensors. The key benefits of this structure include high sensitivity and selectivity to glucose, as well as the ability to reuse the electrode multiple times[26].The dendritic Cu-Ni structures based on graphene offer a large active surface area, making them highly sensitive for detecting even low concentrations of glucose. This property makes them ideal for precise glucose measurements in nonenzymatic glucose sensors[27].These tubular CuS nanocomposites are specifically designed for glucose fuel cells. Their unique structure enhances catalytic efficiency and stability, especially during the glucose oxidation process[28].These TiO_2/Gd_2O_3:Fe photo catalysts, optimized at high temperatures, demonstrate excellent ability to break down pollutants when exposed to UV light, thanks to their specialized structural properties[29].Calcium-zinc oxide nanoparticles are gaining attention for their potential in optoelectronic applications due to their unique conductivity and complex behavior. With their semiconducting properties and large surface area, these materials are perfect for use in optical devices and sensors[30].Manganese-dysprosium oxide nanocomposites show enhanced photocatalytic activity under UV light, effectively breaking down pollutants. These materials are ideal for environmental applications like water and air purification[31].This work is focused on the synthesis and characterization of a MOF-based nanomaterial for glucose sensing. Herein, the synthesized material is termed

LA@ZIF-8, a ZIF-8-based MOF nanomaterial that includes lanthanum. It is to be utilized for the design and construction of a microscale electrochemical sensor, featuring a three-electrode system on a chip sans the use of enzymes. The sensor would then be applied in the detection of glucose upon the performance of various electrochemical tests, including, but not limited to, cyclic voltammetry and amperometry. Especially, ZIF-8 had a very special tunnel-like structure with a highly porous surface that could offer the best exposure of metal ions as catalytic active centers for ensuring high sensitivity and low detection limits. Accordingly, the compatibility of the pore sizes of the MOF framework and glucose molecules makes possible the "molecular sieving" effect during detection, hence enhancing selectivity. This method hereby adopted to enhance the performance of the non-enzymatic glucose sensor is novel. The multiple valence states and active outer electrons further contribute to the strong catalytic activity, stability, and durability of the sensor with lanthanum. It can, therefore, effectively coordinate with ZIF-8 and enhance oxygen adsorption on its surface, hence fastening the rate of oxidation-reduction reactions. Besides, lanthanum increases the current density, hence amplifying the performance of the glucose sensor. However, all the mentioned properties of the synthesized materials are by order of magnitude tremendously higher compared to the materials without lanthanum or those which have not been able to employ MOF nanomaterials as catalysts for glucose detection. The microstructural characteristics of LA@ZIF-8 significantly influence its electrochemical properties. This compound features a Zeolitic imidazole framework (ZIF-8) that boasts a high surface area and small nanoparticle size, which together increase the number of active electrochemical sites, thereby enhancing the sensor’s sensitivity. The porous structure of ZIF-8 facilitates easier access for the electrolyte and target molecules to these active sites, which

accelerates the electrochemical reactions. Furthermore, the inclusion of the LA compound (for instance, lanthanum oxide or another related compound) within the LA@ZIF-8 structure is crucial for improving the electrocatalytic properties of the sensor. The presence of LA acts as a catalytic enhancer, promoting electron transfer and reducing the internal resistance of the sensor, which in turn boosts current and sensitivity. Additionally, the shape and arrangement of the microstructure in LA@ZIF-8 facilitate electron transfer and help prevent electron buildup on the sensor surface, which enhances both stability and reproducibility. The structural order within LA@ZIF-8 contributes to reduced electrical resistance and long-term stability, ensuring that the sensor retains its performance across different conditions

2. Experimental section

2.1. Materials and Reagents

Zinc nitrate, 2-methylimidazole, lanthanum nitrate, silicon dioxide, fluorosilicate SU-8, polydimethylsiloxane (PDMS), polyethylene terephthalate (PET), potassium hydroxide, glucose powder (The glucose used in our research was received from a famous medical center, Social Security Hospital, Tehran, Iran. We received it in a normal, sterilized powder form through the laboratory of the hospital), gold ink, Rogers substrate, Plexiglas, and dimethylformamide (DMF) ink were prepared from Sigma-Aldrich, USA, and Merck, Germany.

2.2. Equipment

The morphological feature examination of doped porous carbon Lanthanum@ZIF-8 was done by a scanning electron microscope (SEM), SUPRA-55VP ZEISS, manufactured in Germany, which was supported by Energy dispersive X-ray spectroscopy. A micro fabricated sensor was designed

and constructed for all electrochemical and amperometry monitoring. The sensor is made up of a main channel and a reference channel, with a 3-electrode system consisting of a reference electrode, a counter electrode, and a working electrode in gold. Doped porous carbon Lanthanum@ZIF-8 (5 mL) was cast onto a Gold electrode (AUE) for use as the working electrode in 0.1 M potassium hydroxide (KOH) solution at room temperature.

2.3. Electrocatalyst preparation

This work presents an empirical investigation through a facile synthesis procedure into a new electrocatalyst using metal-organic framework nanomaterial. Figure 1 represents the synthesis methodology followed in this work, along with the operational parameters. The prepared sample was subsequently carbonized in a furnace under the following conditions

2.3.1. Synthesis and preparation of ZIF-8

Synthesis of La@ZIF-8 powder: 2268 mg 2-methyl imidazole and 1188 mg zinc nitrate were each dissolved in 60 mL methanol with ultrasonication treatment for 20 min to get transparent solutions.

In the second step, the addition of the first solution into the second one was made. The final mixture was continuously stirred at 35°C for 6 h using a magnetic stirrer to form ZIF-8. Centrifugally separated product was then washed with methanol and dried overnight in a vacuum at 60°C.

2.3.2. Synthesis and preparation of La@ZIF-8 NPC

0.90g of ZIF-8 powder was dispersed into 100ml of methanol by ultrasonication for 15min. Then, 1.3g of lanthanum nitrate powder was added to the above solution and sonicated for 15min. The pH value adjustment was appropriate. Finally, continuous stirring using a stirring rod

was carried out till the end. Product was washed three times with deionized water and then centrifuged and dried in a vacuum at 80℃. Derived carbon: The La@ZIF-8 powder was put into the ceramic tube furnace and treated under AR gas flow at 900℃ for 3 h and then cooled to room temperature. Preparation of Catalyst Ink: Firstly, 1 mg La@ZIF-8/NPC was dispersed in 1 mL DMF solution and then ultrasonicated for 15 min.The resulting catalyst ink (5 μL) was dropped onto the working electrode firstly polished with alumina (Al2O3), then washed with ethanol and ultrapure water, and dried in air at room temperature. Figure 1 presents the preparation process diagram.

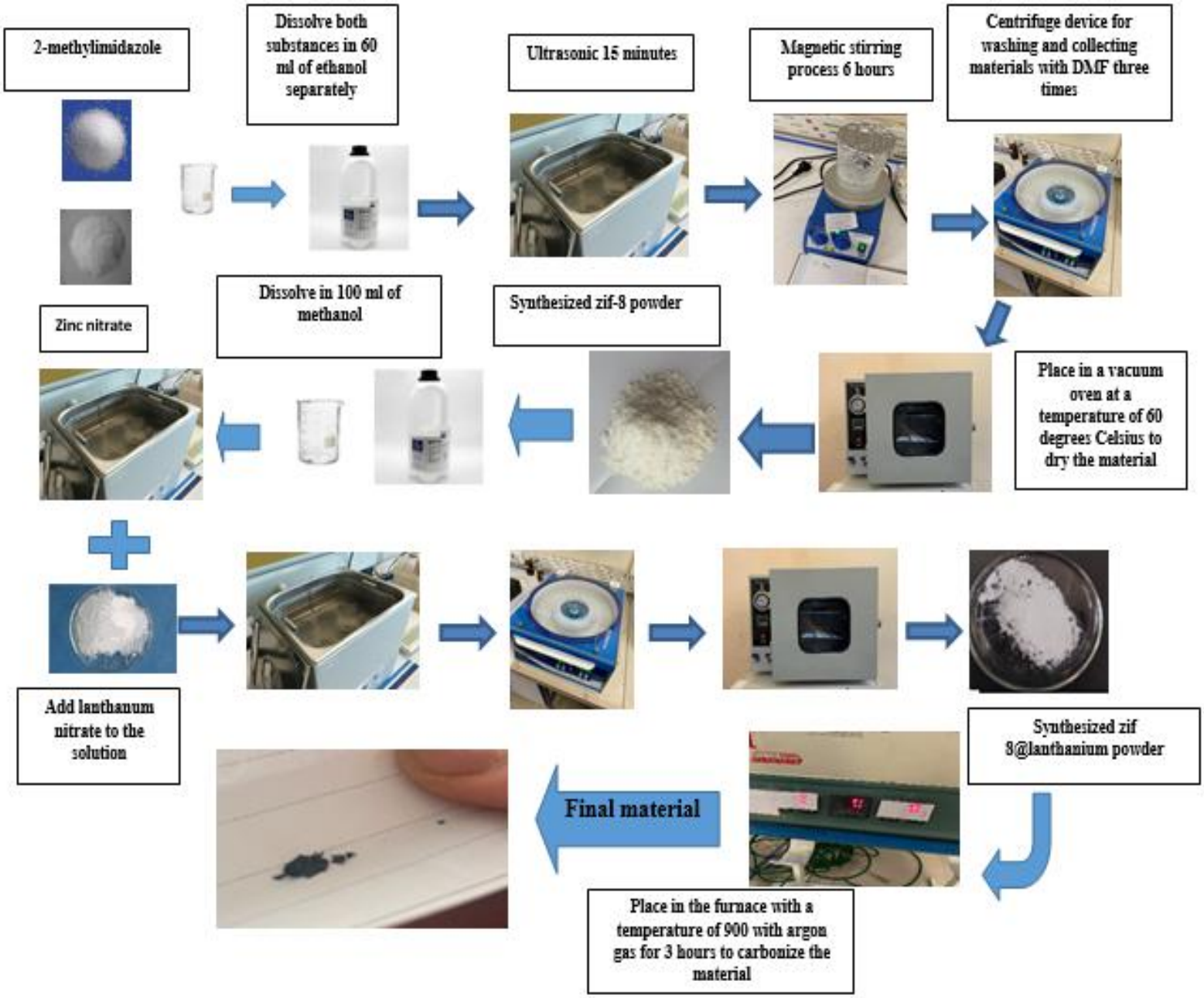

Figure 1. Stages of catalyst sensor fabrication

2.Characterization Tests

For the purposes of this study, the physical aspects of the produced electrocatalysts were characterized using different techniques. With the assistance of Scanning Electron Microscopy (SEM), it was possible to image the samples at a great resolution greater than that achieved with the optical microscope by several hundred thousand times and determine the surface texture of the surfaces. SEM and Energy Dispersive X-ray Spectroscopy (EDS) were used in combination to locate and measure surface areas on solid samples after they had been prepared. This is based on compositional analysis of the sample by means of X-ray energy emitted from the sample, and measuring the type and amount of each element present in the sample [16]. Such an analysis was carried out using the EDS "SAMX" device produced by SAMX from France.TEM analysis, or Transmission Electron Microscopy, is one of the most important methods for studying materials, especially nanostructured materials, due to its high imaging capacity of nearly one million times magnification[17] With the TEM analysis, it is possible to see variations in the nanostructure of materials and the shape of nanoparticles including the structure of those within the particles such and core shell atoms. Philips EM208S 100KV 100KV device manufactured in the Netherlands has been employed for the purpose of TEM analysis. However, while analyzing. By examining the XRD output spectra, which are recognized as X-ray diffraction patterns, the crystalline structure, grain size, atomic spacings, lattice parameters, and crystal defects can be studied The XRD STAD IP instrument with capabilities of normal + high-angle (from angle 5-100 degrees) was utilized for this purpose. Infrared transform microscopy (FTIR) incorporates the use of spectroscopes for compound identification in both organic and mineral materials. This is, however, an analysis technique that is partially reliant on other spectroscopic techniques. Within the framework of FTIR microscopy, the sample molecules are quantitatively analyzed for their

absorbed infrared rays. For this analysis, an FTIR Spectrum1 device having 400-4000 cm-1 FTIR Capability, ATR 600-4000 cm-1, and a solution of acid and organic compounds was used[19].Besides FTIR spectrophotometry, Raman spectra analysis is highly regarded, as the technique can also be used to accurately evaluate molecules and their structural characteristics, evaluate the bonds formed, and understand the substances in detail. Fusion of some bonds in materials is more clearly detectable in Raman while other bonds show better resolution in FTIR[20]. Many carbon nanotubes, fluorine, and graphene are GIT arrangements and the Raman test is expedient to evaluate carbon structures at the GIT stage. We used the Takram P50C0R10 device, produced by TEKSAN, powered by a 532-nm laser with a laser beam intensity of 0.5 to 70mW [18].

3.1. Characterization and Morphology Studies

Scanning Electron Microscopy (SEM) is an appropriate technique in both the imaging of nanostructures and chemical composition identification. SEM is the only instrument in this regard that exploits the surfaces of materials more decisively than optical microscopes. In particular, SEM has the ability to create three-dimensional images of the sample structure by a focused beam of electrons. In the image depicted in Figure 2a ZIF-8 particles also display a more regular form, whose size is about 1-2 micrometers. These particles have smooth surfaces and comprise transparent crystalline units. La@ZIF–8 demonstrates, as shown in Figure 2b, that the surfaces of those particles are rough, but the cage-like formation is still intact. In addition, with an increase in temperature the particle size decreases, more noticeably at the highest temperature of 900°C and in this way smaller particles containing higher specific surface areas can be

produced. La@ZIF-8's particulate nature is further confirmed by the apparent hollow structures in the TEM image of La@ZIF–8 presented in Figure 2c.

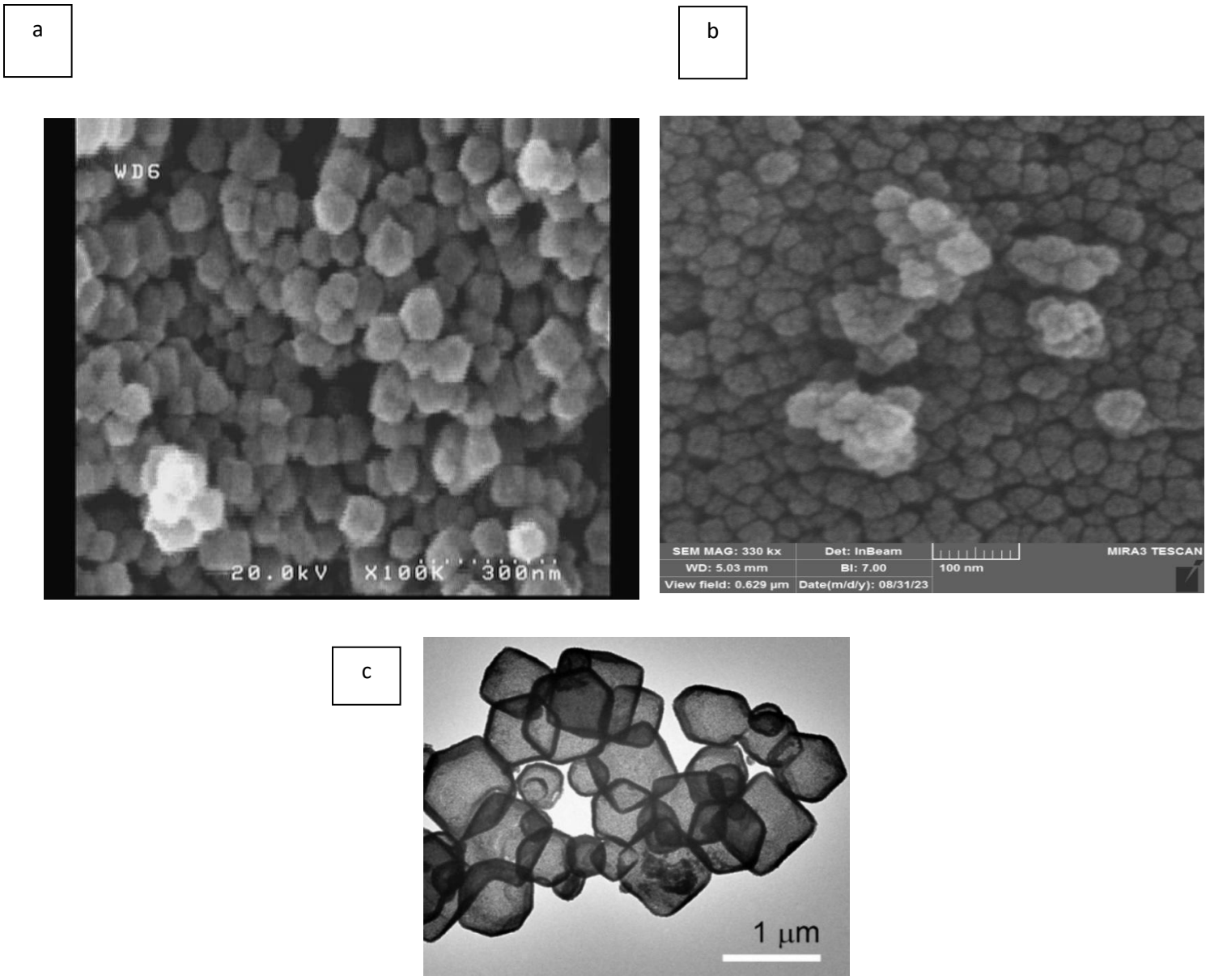

Figure 2. SEM-TEM images: a) SEM image of ZIF-8 particles.b) SEM image of La@ZIF-8 derived at 900°C.c) TEM image of La@ZIF-8 derived

The EDX analysis in Figure 3 illustrates structures of La@ZIF-8 while indicating the elemental presence of carbon, oxygen and lanthanum. Further, the elemental CMOF composition as EDS determined, confirms above the successful purification of ZIF-8. The ZN signal arises from a TEM grid. Alan@ZIF-8/NPCsample was synthesized electing Figure 3a to find the composition. Figure 3b demonstrated that the EDS analysis of La@ZIF-8/NPC revealed the presence of N, C, O, La, and Zn. Since carbonization of the material in the furnace increased the number of carbons

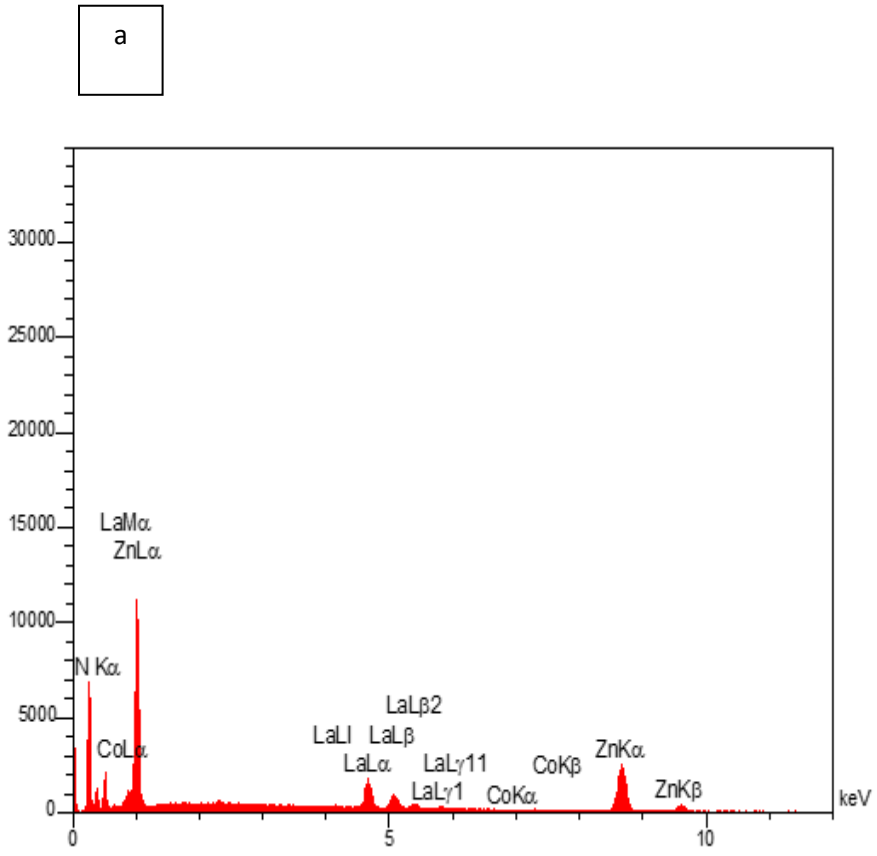

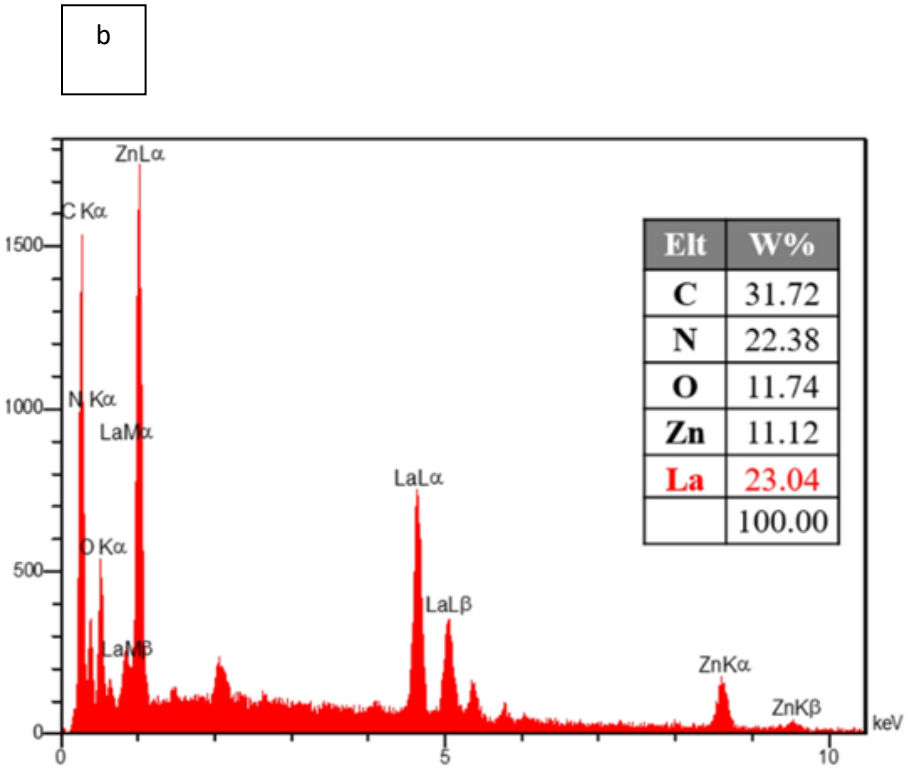

Figure 3. EDX analysis: (a) before NPC, (b) after NPC.

To examine the obtained crystal structure, XRD analysis was conducted. Figure 4a shows the XRD pattern of ZIF-8 nanoparticles. The sharp peak at 7.2 degrees indicates the highly crystalline nature of ZIF-8 nanoparticles, aligning well with the standard graphite pattern. Figure 4b depicts the XRD analysis pattern for ZIF-8/NPC at a furnace temperature of 800 degrees Celsius, and Figure 4c shows the XRD analysis pattern for La@ ZIF-8/NPC at temperatures of 800 and 900 degrees Celsius. It is evident that with an increase in furnace temperature, sharper and better-defined peaks are observed at 26.61 and 43.45 degrees, corresponding to the (002), (100), and (110) crystal facets of graphite, respectively, consistent with the standard graphite peaks (JCPDS No. 01-075-2078). No impurity peaks were found, indicating the high purity of the obtained La@ ZIF-8material.

. Impact of Lanthanum Loading: A comparison of the XRD patterns(B,C) shows a reduction in the intensity of certain peaks after lanthanum is loaded, while the main structural peaks remain

unchanged. This suggests that the crystal structure of ZIF-8 is maintained even with the addition of lanthanum. Structural Integrity of the MOF The coordination network between zinc ions (Zn^{2+}) and dimethyl imidazole ligands appears unaffected by the lanthanum incorporation, indicating that the fundamental ZIF-8 structure is preserved. Formation of Lanthanum nitride In the lanthanum-loaded sample, additional diffraction peaks align with the standard pattern for lanthanum nitride as specified by JCPDS 36-1481. This observation confirms that the lanthanum is present in the material

a

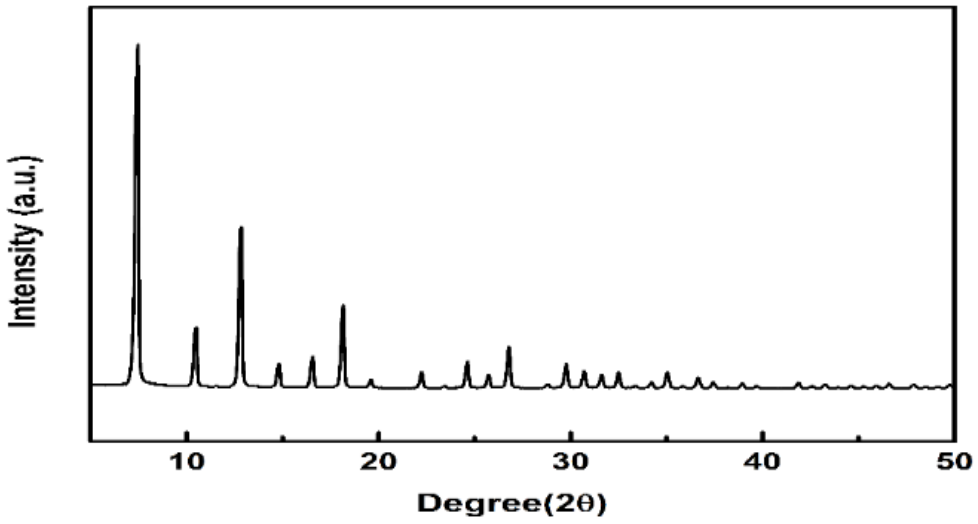

b

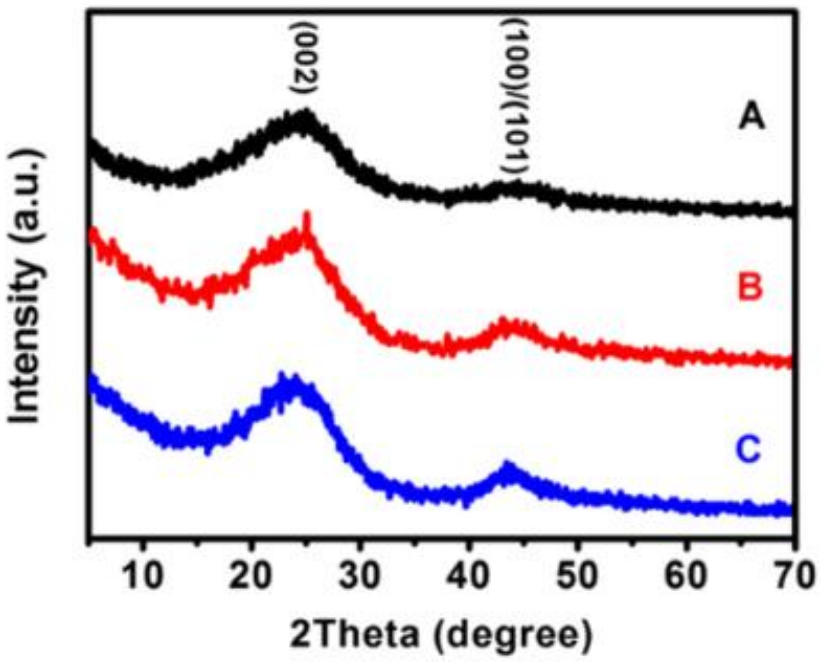

Figure 4. XRD pattern of ZIF-8 nanoparticles and ZIF-8/NPC pattern at 800 degrees Celsius furnace (A) .La@ZIF-8/NPC pattern at 800 degrees Celsius furnace (B). La@ZIF-8/NPC pattern at 900 degrees Celsius furnace (C).

Raman scattering or the Raman effect is a particle inelastic two photon process. When the sample undergoes Raman scattering, the orientation polarizability is altered by the vibrational motion of the molecule. Molecules interact with laser light by means of Raman scattering yielding a Raman spectrum associated with the polarizability of the molecule. A technique, Raman spectroscopy that explores this phenomenon investigates samples to deduce intra molecular bondings and gives out different Raman spectrums for different molecule structures.

In Figure 5:Curve A is the Raman spectrum of ZIF-8 at 1800 °C.The Raman spectrum of La@ZIF-8 at 800 °C is represented by Curve B.The Raman spectrum of La@ZIF-8 at 900 °C after furnace treatment is shown on Curve High intensity for La@ZIF-8 at elevated temperature of 900 degrees Celsius is revealed at 1200 cm^-1 for D band and 1630 cm^-1 for G band. The D

band reveals disorderliness of carbon and irregular carbon areas, whereas the G band reveals orderliness of sp2 carbon and points to graphitic carbon in all samples. The relative intensity ratio I_D / I_G state at 900 degrees Celsius is 0.73, so that temperature promotes the degree of graphitization.

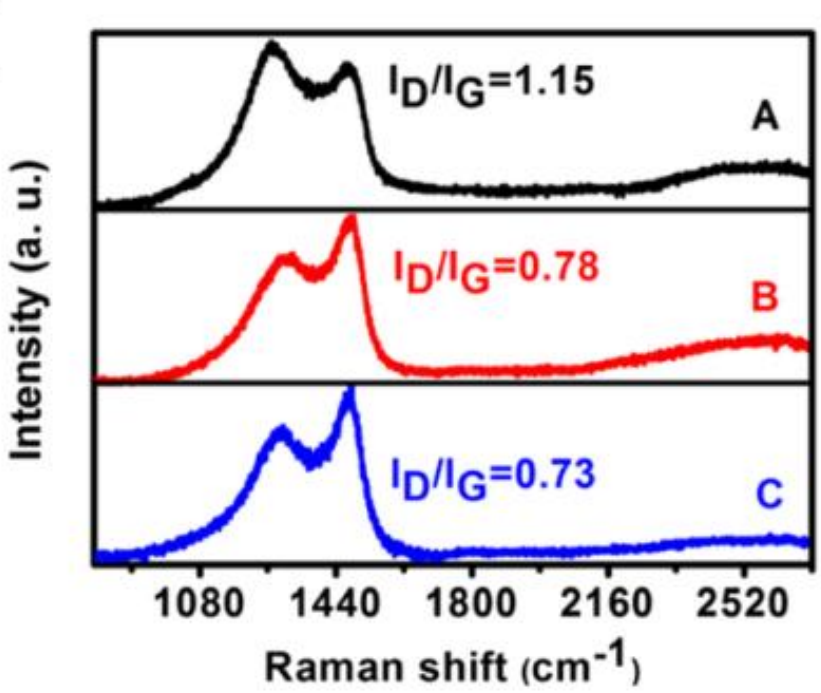

Figure 5. Raman spectrum pattern for ZIF-8/NPC at 800 degrees Celsius furnace (Curve A). Raman spectrum pattern for ZIF-8@LA/NPC at 800 degrees Celsius furnace (Curve B). Raman spectrum pattern for ZIF-8@LA/NPC at 900 degrees Celsius furnace after furnace treatment (Curve C)

In Figure 6, FTIR spectrum of the obtained La@ZIF-8 after carbonization at 900°C is demonstrated. Bands near 3327.6 cm^-1 are attributed to very intense O-H carboxylic bond stretching. Bands at 1992 and 2017 cm^-1 can be dotted to normal stretching of C=C bonds. The band at 2198 cm^-1 is

contributable to under damped vibrating of C≡C bond. The band observed at 2920 cm^-1 is attributed to an asymmetric stretching of aliphatic C-H groups. A shoulder at 1704 cm^-1 can be attributed to carbonyl groups. Characteristic 700-500 cm^-1 range is for the suitable stretching of five-membered heteroaromatic rings with double bonds. Absorption bands in the regions of 700–800 cm^-1 may be due to the presence of hydrogen in five-membered heterocycles containing CH=CH fragments. Bands at 901 and 955 cm^-1 are assigned to C=C stretching and band at 1050 cm^-1 represents strong stretching of CO-O-CO. It shows bands at 1243 and 1310 cm^-1 assigned to C-O stretching, 1411cm^-1 to S=O stretching and 1583 cm^-1 to N-O stretching. where the existence of carbon materials in the La@ZIF-8/NPC has been established through this spectrum.

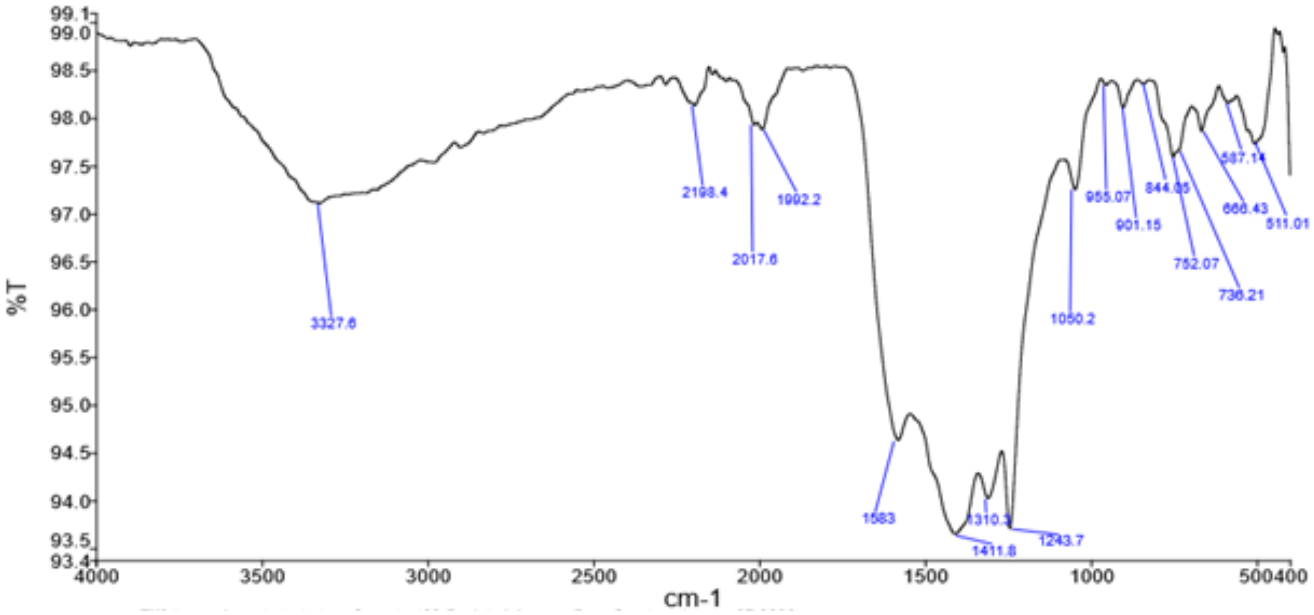

Figure 6.FTIR analysis

4. Electrochemical Testing

The efficiency and properties are determined with the Autolab apparatus to evaluate characteristics of the sensor. In this device, the processes such as cyclic voltammetry which involves oxidation and reduction on the specified sensor and chronoamperometry involving the measurement of current are performed. The equipment used in this sort of analysis requires only a three-electrode system that include; working, reference and counter electrodes which are made of gold and mercury. The steps include placing the synthesized exact quantity of catalyst to the working electrode and drying it under red neon lamp. Then, a prepared glucose-containing solution is added, followed by immersing the previously standardized three-electrode system into the solution for purpose of sensor identification. In all cyclic voltammetry (CV) tests, the x-profiles of the potential axes were adjusted with regards to the reference electrode.

4.1. The electro-catalytic glucose oxidation on the La@ZIF-8/NPC/AUE

hybrid electro-catalyst was investigated in 0.1 M phosphate-buffered saline (PBS) containing 10 mM glucose at a scan rate of 50 mVs [1]To analyze the electrochemical performance of electrodes related to the oxidation of glucose, the analysis is done in a 0.1 M KOH environment with and without 0.1 M glucose concentration using CV measurements in the potential window of 0-0.8 V at the a scan rate of 100 mV/s as shown in figure 7. However, no redox peaks of the bare AUE are observed in both the absence and presence of 0.1 M glucose, indicating the inability of glucose oxidation on the bare AUE surface as represented by curve 1 and curve 2.From the curve (3) with 0.1 M glucose in a 0.1 M KOH, we can clearly conclude that La@ZIF-8/AUE can show a redox couple and La(II)/La(III) conversion in the alkaline environment. For the modified electrode, the deposited lanthanum exhibits a pair of quasi-reversible redox peaks, where the oxidation process is associated with the electrochemical reactions of La(II)/La(III).After that,

curve (4) describes that La@ZIF-8/NPC/AUE, all through, provides the highest and the most eminent reduction surge. This observation suggests that the deposited catalyst on the NPC sheets supported on the GCE surface performs better than other electrodes. This is due to the improved characteristics of the upgraded lanthanum ions and N-doped carbon dots, which give the most efficient method to the quantitative measurement of glucose in biological fluids and in real-world samples. Therefore, it is reasonable to suggest that the La@ZIF-8/NPC nanoframeing construct indeed provides the most efficient electrochemical transfer.

$$L\ (II)_{La\text{-}Mof} + 2OH^- \rightarrow La(III)_{La\text{-}Mof} + e^- \quad (1)$$

$$La(III)_{La\text{-}Mof} + glucose \rightarrow La(II)_{La\text{-}Mof} + gluconate \quad (2$$

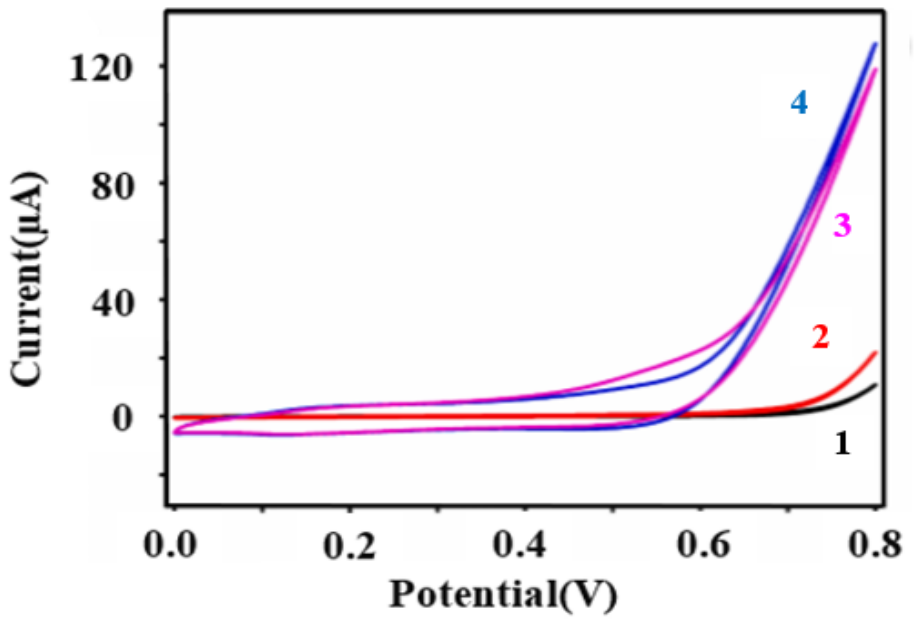

Figure 7.The redox peak in the presence or absence of glucose (curves 1-2) indicated no significant activity. The redox peak related to ZIF-8/NPC is shown in curve (3), and the redox peak related to La@ZIF-8/NPC is shown in curve (4).

4.2. Impact of Glucose Concentration with the Modulation of Scan Rate

To study the influence of concentration changes, different glucose concentrations (0-6 mM) injected and the potential range 0-0.8 V as well as the scan rate of 100 mV/s were used. As shown in Figure 8, the CV of La@ZIF-8/NPC/AUE in 0.1M PBS containing different concentrations of glucose (0mM, 2mM, 5mM) has been presented. There is clear trend showing that as glucose concentration increases so does the reduction current which suggests that glucose can be oxidized and reduced at the same time. The present experiments show that incorporation of glucose in La@ZIF-8/NPC/AUE has the maximum anodic peak development potential.

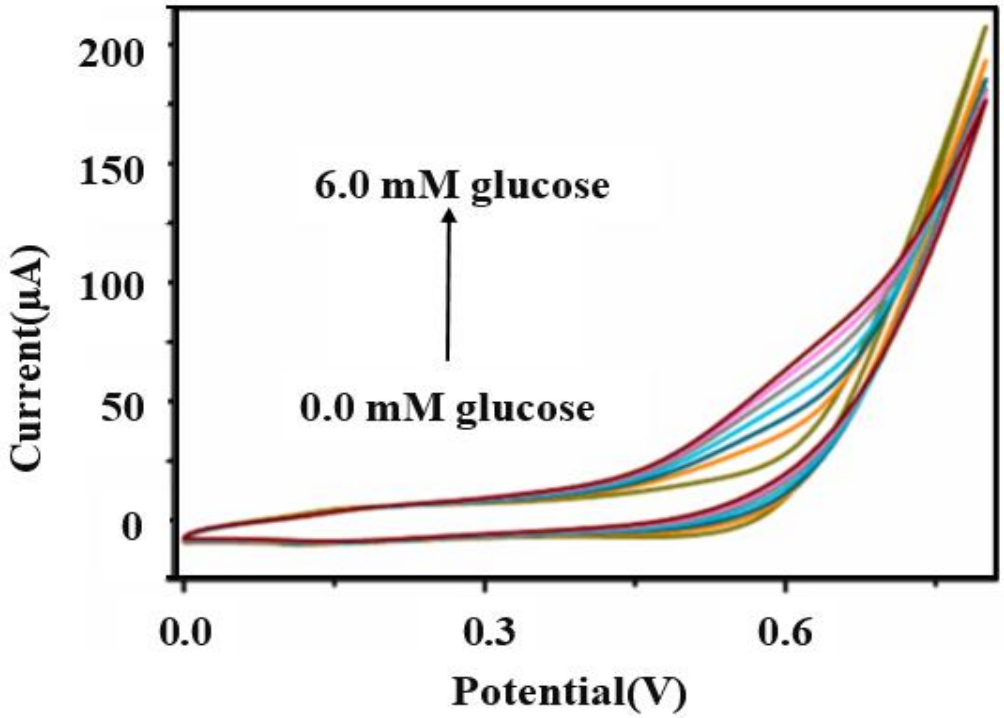

Figure 8. Redox peak of La@ZIF-8/NPC based on a constant scan rate and varying glucose concentrations (0-6 mM).

4.3. Effect of Scan Rate Variation and Constant Glucose Concentration

To test the influence of the scan rate, cyclic voltammetry of La@ZIF-8/NPC/AUE in 0.1M KOH containing 0.1M glucose was performed at scan rates ranging between 20 and 200 mV/s in a range of 0-0.8 V (Figure 9). When increasing the scan rate, both anodic and cathodic peak currents were found to be increasing proportional to the scan rate, with a correlation coefficient of 0.9993. A controlled electrode process was established by the relative increase in both cathodic and anodic peak current resulting from the increase in scan rate.

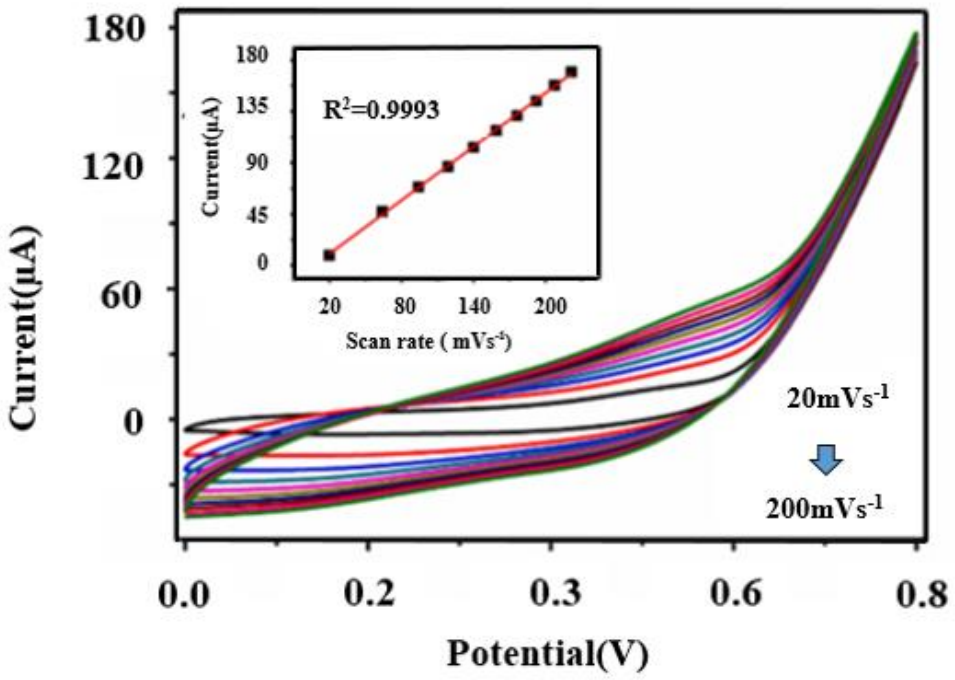

Figure 9. Cyclic voltammetry diagrams based on a constant concentration of 0.1 M glucose in 0.1 M potassium hydroxide and a variable scan rate (20-200 mV/s).

4.4. Glucose Detection by La@ZIF-8/NPC/AU-Electrode Amperometry Response

An optimal potential of 0.55 V was selected for glucose detection. To study the effect of glucose detection, La@ZIF-8/NPC/AU-Electrode in 0.1 M KOH was examined using amperometry (i-t) experiments with increasing concentrations of glucose at an optimal potential of 0.55 V under magnetically stirring conditions, as shown in Figure 10a. The amperometry responses of La@ZIF-8/NPC/AUE to successive additions of glucose concentrations exhibit high performance with rapid response times of 0.9-1.7 s, indicating that the non-enzymatic glucose biosensor has a fast and extremely sensitive response. Figure 10b shows the ΔI of the working electrode with the addition of varying glucose concentrations, demonstrating that ΔI significantly increases as glucose concentration increases, and then the peak current gradually deviates from the linear range. The amperometry calibration of varying glucose concentrations in the linear range of 0-6950 μM shows a correlation coefficient of R^2 = 0.9960 Compared to other non-enzymatic glucose sensors, La@ZIF-8/NPC/AUE exhibits a low detection limit of 0.2 μM (S/N = 3) and a very high sensitivity of 30,000 μA mM^{-1} cm^{-2}**.**

a

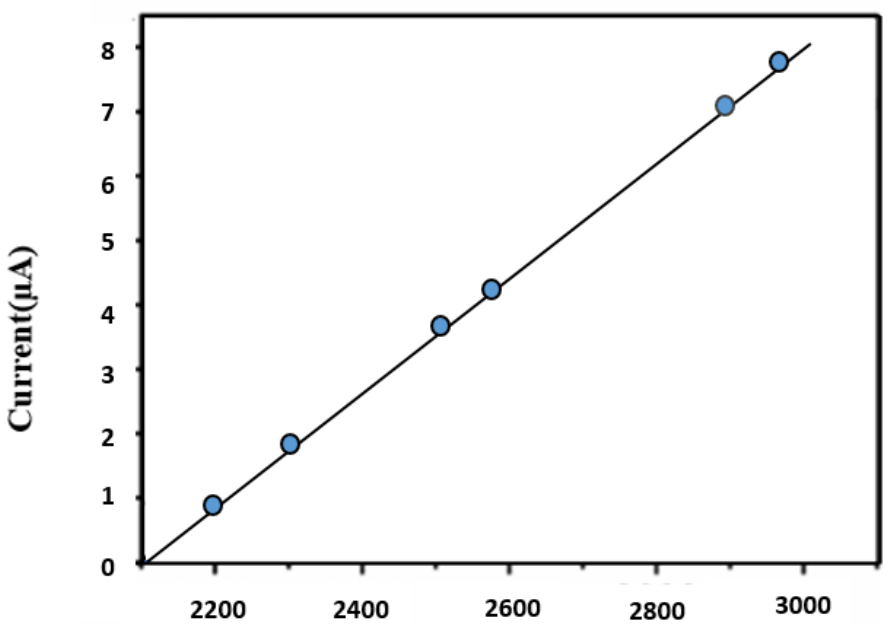

b

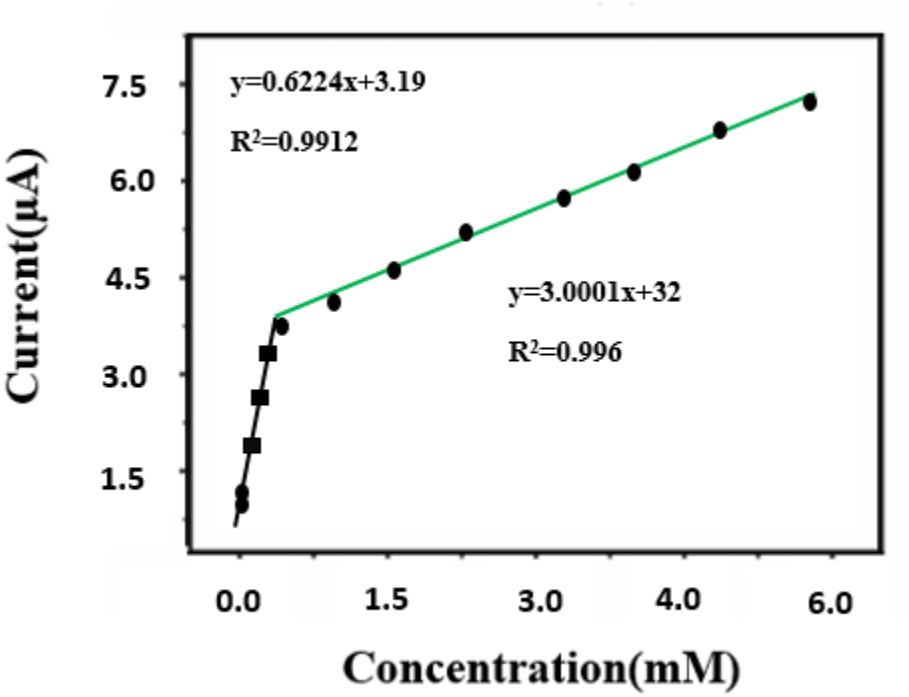

Figure 10.(a) Linear graph of current changes over time based on concentration changes.(b) Linear graph of current changes over time based on concentration changes.

5. Sensor Construction

Herein is explained the method of creating a three-electrode system and a microfluidic glucose detector**.**

5.1. Design and Fabrication of Electrochemical Microscale 3-electrode System for Glucose detection

5.1.1. Microscale 3-Electrode System Design Using AutoCAD Software:

In AutoCAD software the preliminary plan for fabrication of the system contains three electrodes and a micro scale chip with two channels. The drawing which you see in the picture below was drawn on the drawing plane of AutoCAD based on the required dimensions. The size of the Rogers substrate for the electrode printing was determined to be 3cm x 4 cm. It is shown in Figure 11**.**

5.1.2. Electrode Design

The interdigitated microscale working electrode, the reference electrode, and the counter electrode were designed and printed on the Rogers substrate using PEDOT: PSS gold flexible ink. Their dimensions were considered as follows**:**

5.1.3. Working Electrode Dimensions

• 4 mm x 4 mm: Sizes of both square-shaped pads located at the endpoint of the electrode for current transfer process.

• 230 micrometers: Measured diameter for a portion of the distance from electrode ends.

• 500 micrometers: Length of a first segment of the working electrode for spanning over the synthesized catalyst as well as to immerse it in the glucose containing solution.

5.1.4. Reference Electrode Length

• 4 mm x 4 mm: Sizes of the pad at the end of the electrode with dimensions of a square in reference to current conception.

• 500 micrometers: Thickness of the second portion of the electrode kind adopted in the construction of the sample.

• 4 mm x 5 mm: Sizes of certain segment of the reference electrode for touching a glucose containing solution.

5.1.5. Counter Electrode Dimensions

• 4 mm: Features of the circular plate at the end of the electrode for transmitting current at the end of the pad formed in the shape of a square.

• 500 micrometers: The width of middle part of the strip for the electrode.

• 400 micrometers: Width of the initial part of the counter electrode for contacting the glucose-containing solution

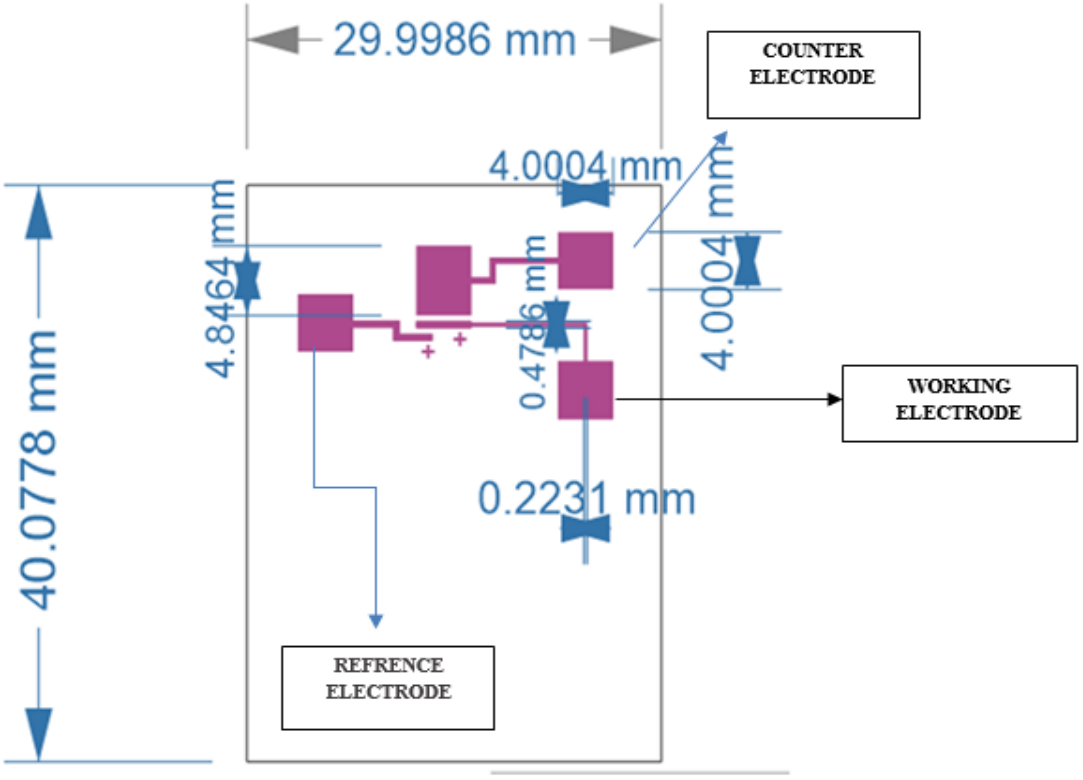

Figure 11. Design image of a 3-electrode system in AutoCAD software

5.1.6. Printing of the Three-Electrode System

Gold The designed three electrode system was prepared using ink and Rogers's plate. The required electrodes were then screen printed on the Rogers substrate. In this process, the computer software offers the St. design to the screen printer and the latter directly and all at once impose the design onto the substrate using the stencil. In this project, the thickness of the printed gold is 10 microns. It is shown in Figure 12.

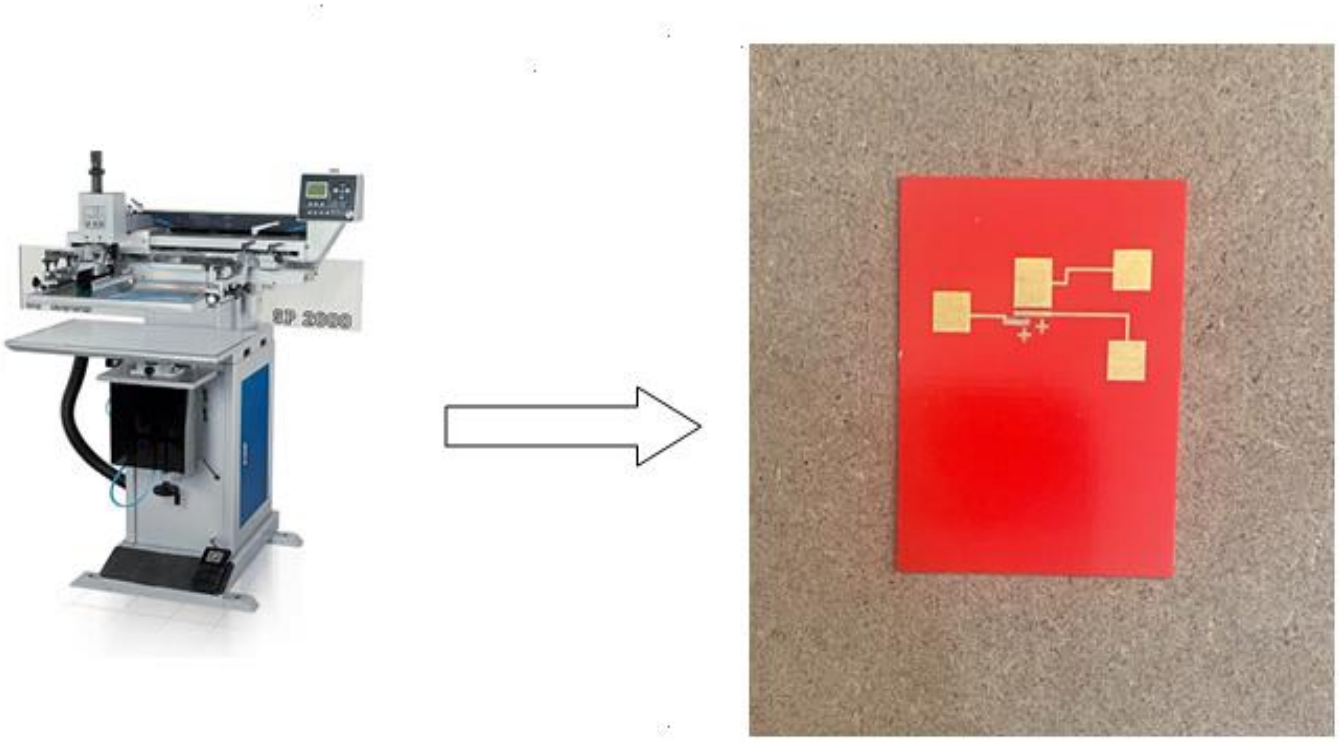

Figure 12. Image of a printed 3-electrode system using a screen printer

5.2. A novel approach for design and fabrication of microfluidic chip for glucose sensor is presented in this section.

5.2.1. Design Microfluidic Sensor with the help of Auto CAD Software

In the microfluidic chip, dimensions of 1.5 cm and 3.5 cm were compassed for the total area of the chip. The designed microfluidic chip had one inlet and two inlets merging into one that formed the outlet. It is shown in Figure 13.

5.2.2. Main Channel Dimensions

• Width: 500 micrometers

• Length: 3 centimeters

5.2.3. The Reference and Subsidiary channel dimensions are not directly reported by an empirical study; rather, they need to be specified and measured in reference to the goods or services that compose the specific channel.

• Width: 90 micrometers

• Length: 0.5 centimeters

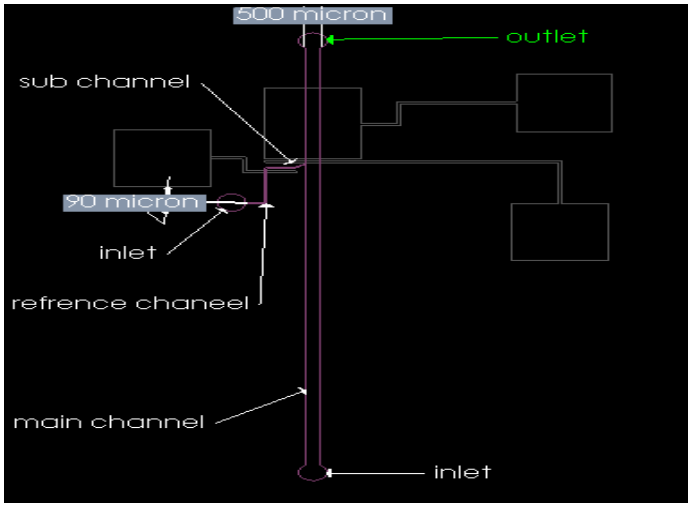

Figure 13. Design image of a channel in AutoCAD software

5.3. Fabrication of Optical Mask

It is sheet having patterned of template which has to be put on the surface of the photosensitive material. The material of the substrate is often transparent and it can be plastic or quartz glass. For this project, the plastic used was transparent type which is scientifically referred to as polyethylene terephthalate, PET. By ink deposition and metal sputtering the desired pattern template is imprinted on the substrate. Their function is to prevent ultraviolet, ion or electron radiation exposure and regulate availability of light-sensitive material according to the pattern. It is shown in Figure 14.

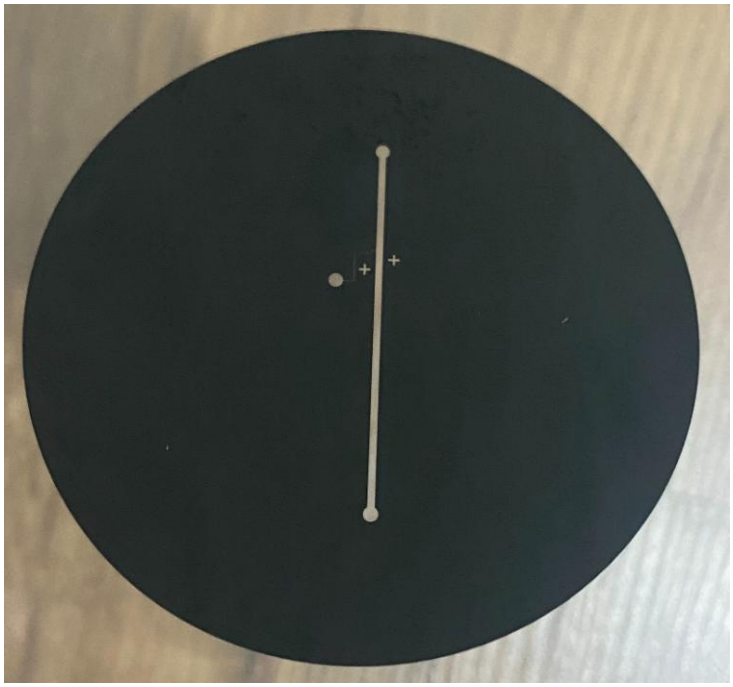

Figure 14. Image of a fabricated optical mask from PET with the desired channel pattern

5.4. Mold Making Steps

Preparation of silicon waver is most commonly used to print out the layout for fabrication of the SU-8 microfluidic chip. Use these procedures to make a template through SU-8.

5.4.1. Wafer Preparation

It does not matter that the wafer is still virgin; it has to be prepared for photoresist. If it is in a cleanroom, wash it with a mix of H_2SO_4 and H_2O_2, otherwise you could wash it with acetone. It is also suggested that moisture should not remain on its surface; hence it can be heated at 120 C for a period of 15 minutes. Moreover, air or oxygen plasma will improve the wetting of the SU-8 on the selected waver by promoting its uniform dispersion. We present Figure 15 of the silicon wafer.

Figure 15.Image of a silicon wafer

5.4.2. Applying Photoresist Layer

The layer of SU-8 2050 negative photoresist is applied to the wafer through the spin-coating to create our future mold. Spin at 1600 rpm for 3 seconds at apply a layer of 100 microns thickness. This is illustrated in figure 16 and Figure 17 above.

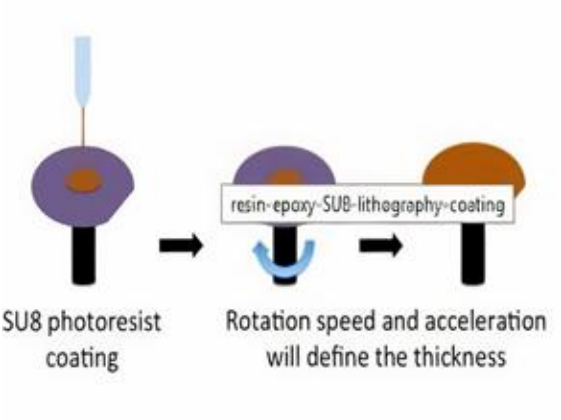

Figure 16. Schematic image of spin-coating process stages.

Figure 17. Image of a spin-coating device

5.4.3. Soft Bake

Treat at 95 degree centigrade for twenty minutes. The soft bake is done to enable the removal of solvent while SU-8 photoresist is being solidified to meet the right consistency for further use. It is shown in Figure 18.

Figure 18. Image of an SU-8 material baking device

5.4.4. UV Exposure

The next step that is taken is exposing the photo images in UV to the baked photoresist area of the mold. The goal of UV irradiation is to harden the photoresist layer and form some solid connections, all of this in the areas where the mask, in its turn, allows the light to shine upon the photoresist surface. Those which remained in the shadow are washed with a solvent. The energy range of UV light used in SU-8 processing is in the range of 365 nanometers only. The exposure time depends on the thickness and power of the lamp Figure19.UV light irradiation.

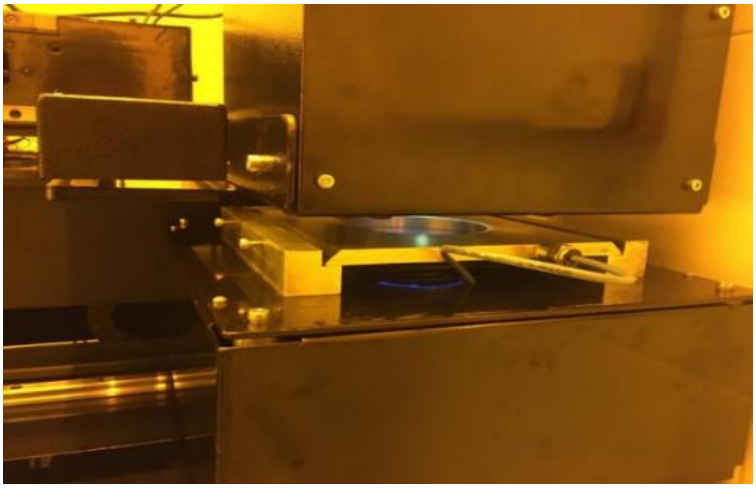

Figure19.UV light irradiation device.

5.4.5. Development

The development stage also referred to as revealing entails the removal of the undesired and unexposed photoresist in a solvent. This is done in order to make the pattern known. Propylene glycol is used for this purpose, and the revealing time takes 1 to 15 minutes for photo resist film depending on the layer thickness of the photoresist. Isopropyl alcohol is used especially in the rinsing of the wafer and the next step will be to blot the wafer with air or nitrogen. Figure 20 and Figure 21 display the impression of the last piece of the template.

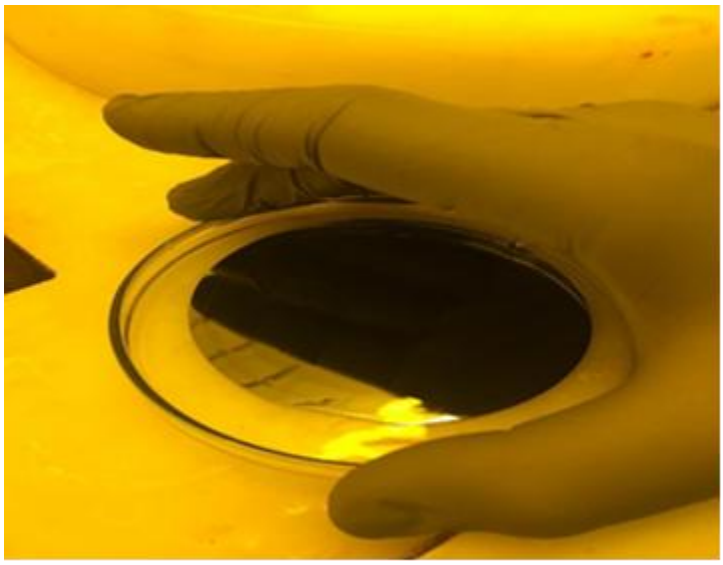

Figure 20. Image of the development stage.

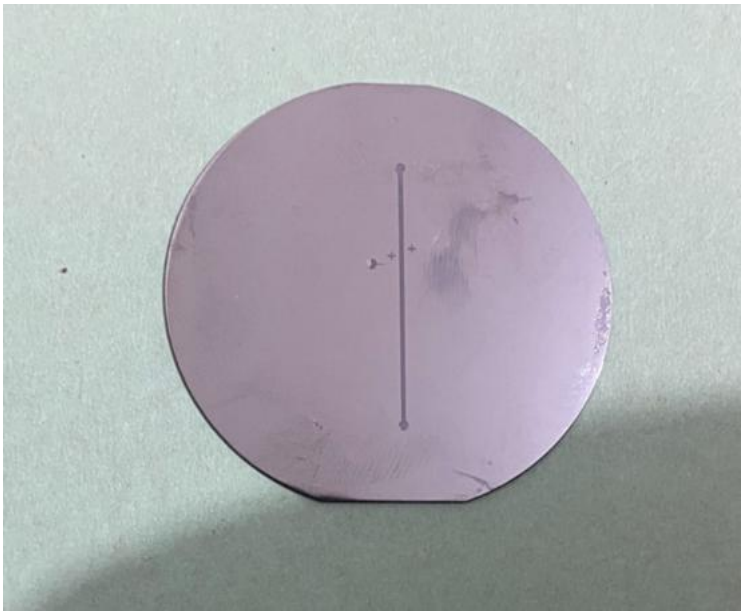

Figure 21. Image of the fabricated mold for the desired microfluidic chip

5.5. Steps for Mold Formation as well as Bonding

Mix Silgard 184 with curing agent at a ratio of 10:1 by weight and then well dispersed in water. Inclusion of curing agent is required for the curing of polydimethyl siloxane (PDMS) because of presence and heat. Silgard 184 is one of the most frequently used polydimethylsiloxane. Here it is also important to add that curing agent should be mixed with PDMS not the reverse way, for curing to take place effectively. It is shown in Figure 22.

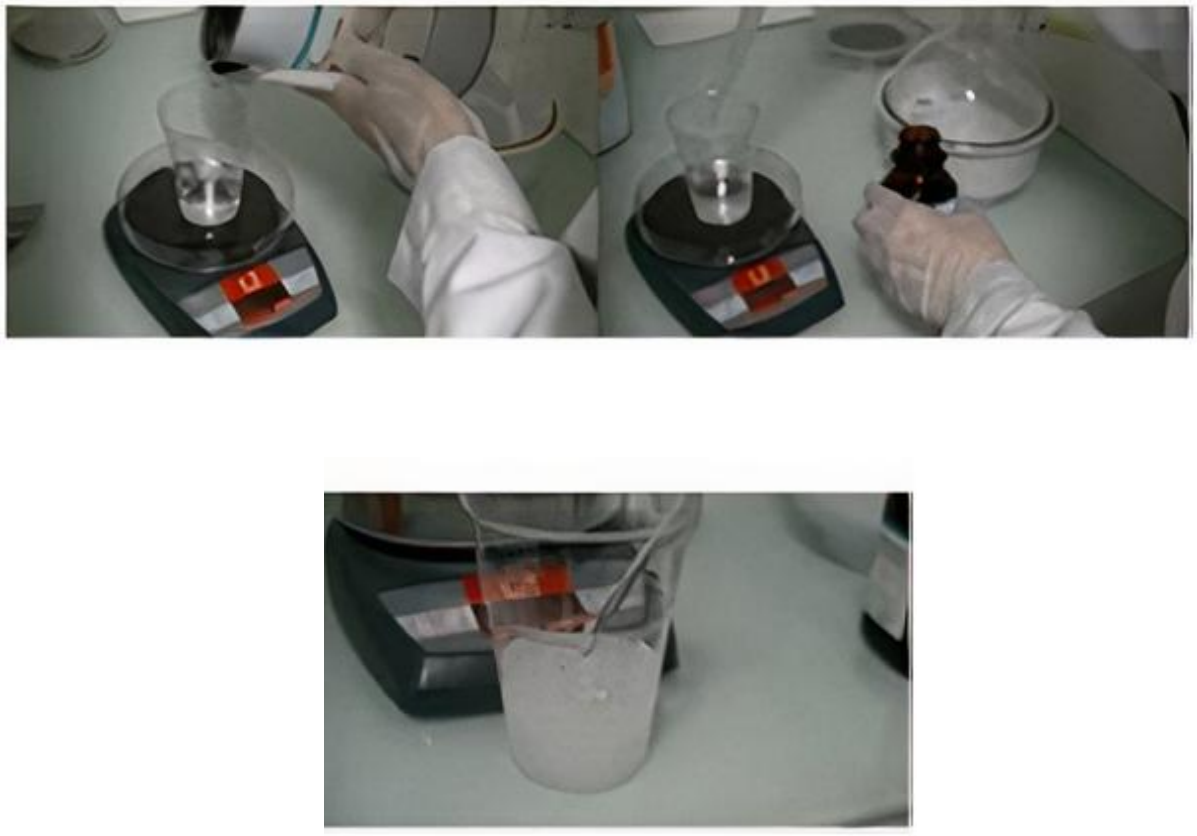

Figure 22. Image of the PDMS and curing agent mixture

5.5.1. Vacuum Degassing

Vacuum degassing for 30 minutes: This stage seeks to get rid of bubbles in the mixture which is made in the previous stage. When the curing agent is added or when mixing is done, it is easy to incorporate air bubbles into the resultant paste. These bubbles are removed by using Vacuum degassing. It is shown in Figure 23.

Figure 23. Image of a disc cutter

5.5.2. After that, the polydimethylsiloxane is poured.

Cast the polydimethylsiloxane mixture into the mold and bake in the hotplate at 90 centigrade for 30 minutes.

5.5.3. Opening the Mold

Finally cut off the polydimethylsiloxane away from the wafer, and punch inlet and outlet hole using 1 mm punch. Figure 24 shows this process. The final assembled image of the electrochemical microfluidic sensor is demonstrated in the figure 25 below.

Figure 24.Image of a punch pen

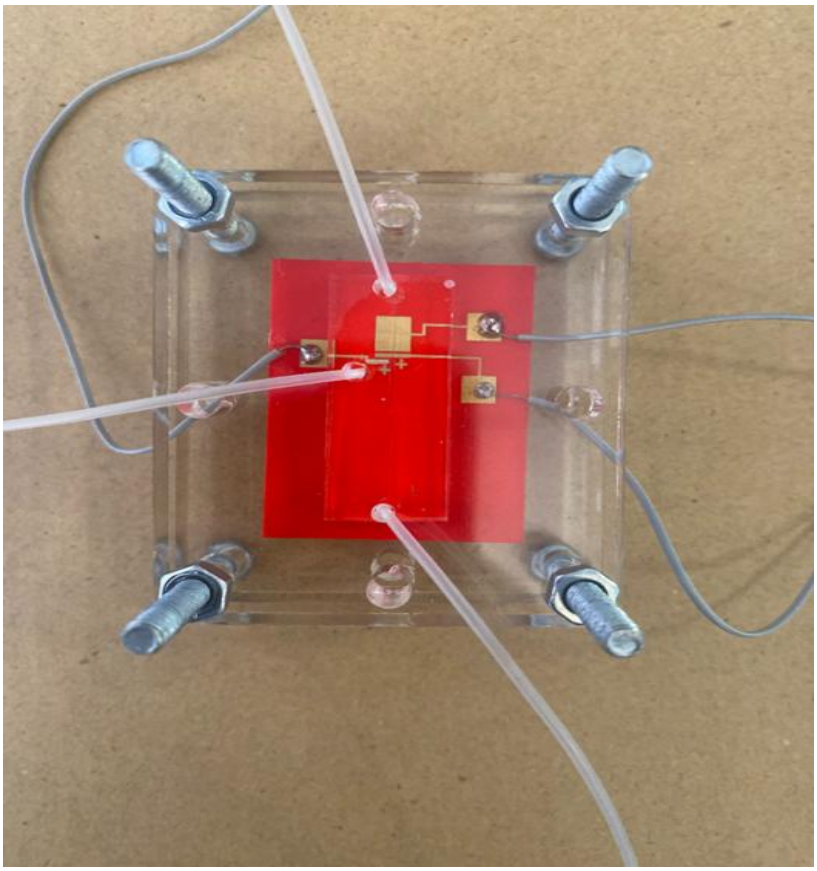

Figure 25. Final image of the electrochemical micro sensor fabricated for glucose detection. The microfluidic chip is securely attached to the three-electrode system with Plexiglas plates and clamps

6. Electrochemical Test

To evaluate the performance of and describe the above sensor, an Auto Lab device is employed. With this device, cyclic voltammetry and chronoamperometry tests are carried out to evaluate the sensor response. In the next step to apply voltage/current and perform cyclic voltammetry and chronoamperometry tests using the Auto Lab device, the wires soldered to the electrode pads are fitted with cables. These wires are also linked to the syringe pump gadget for pumping the mixture of glucose and potassium hydroxide. To determine and assess the performance of the

developed sensor, cyclic voltammetry and chronoamperometry type analyzes will be performed. The results that will be obtained will be presented in the next chapter. This setting has been illustrated in Figures 26 and 27.

a

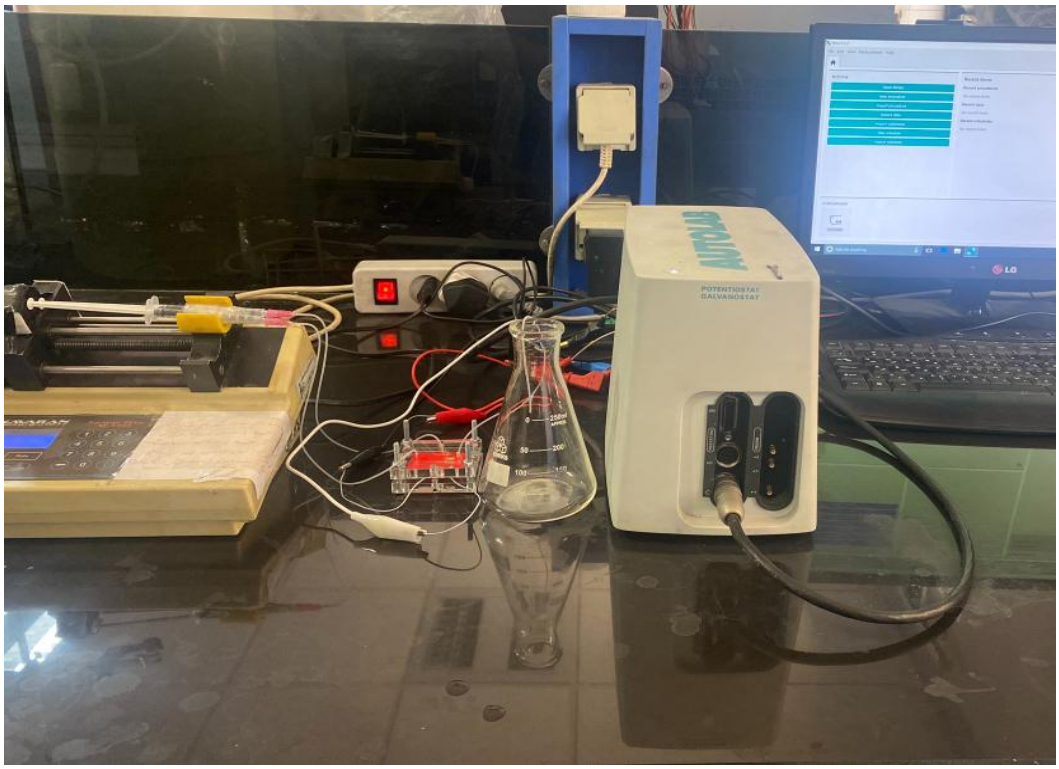

b

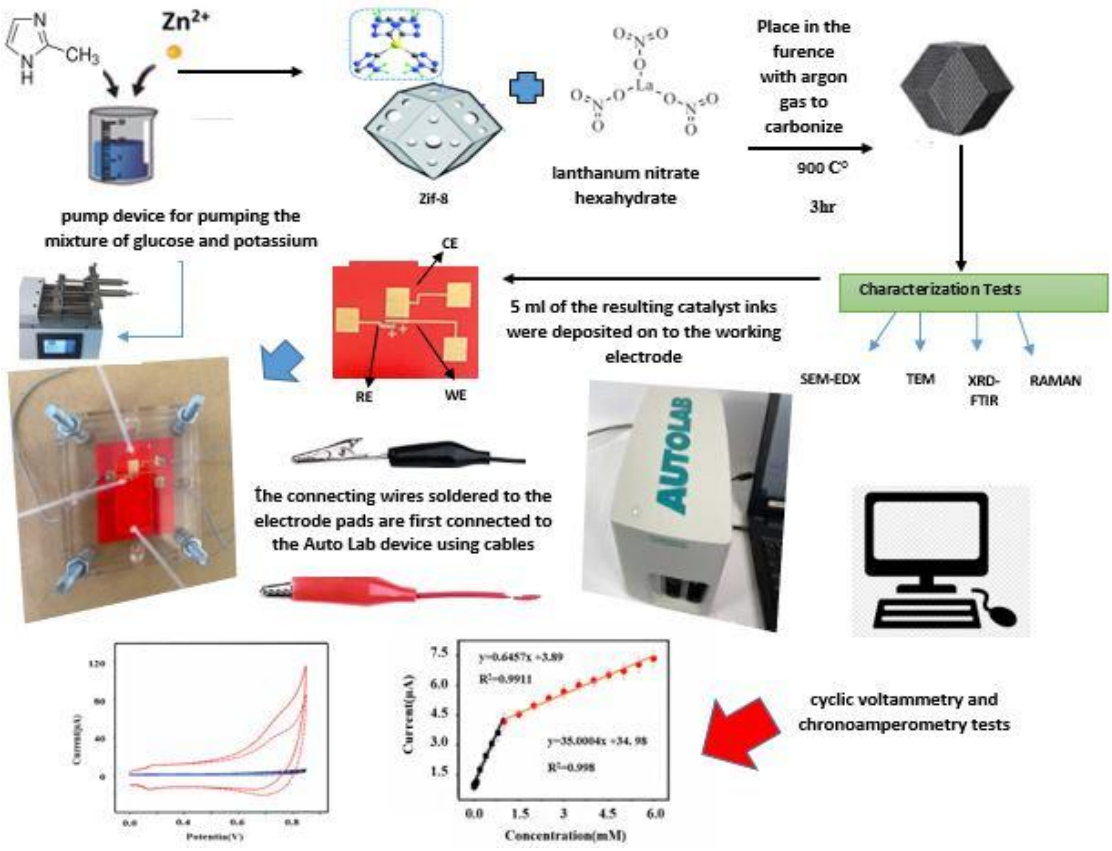

Figure 26. a)Setup used for testing and measuring the output of the micro sensor for glucose detection A b)Microfluidic sensor sensing schematic

6.1. Glucose Electro catalysis by Electrochemical Behavior of Different Catalysts: La@ZIF-8/NPC/AUE

To examine and confirm the electro catalytic behavior of electrodes for glucose detection, cyclic voltammetry experiments were conducted using the Auto Lab apparatus with three catalysts: La@ZIF-8 nanoparticle, as-prepared La@ZIF-8, and La@ZIF-8/NPC were dispersed in a solution with a concentration of 0.1 M glucose and 0.1 M potassium hydroxide. Each sample was used in applying an applied voltage range of 0.8-0 V, and a scan rate of 100 mV/Firstly, uniform catalyst ink of all three materials was prepared by dissolving 1mg of each material in 1 ml of

dimethylformamide (DMF) solution and sonication for 15 min. After that, 5 μL of the obtained catalyst inks were dispensed on the polished WE. Finally the electrode was washed again with aluminum oxide, ethanol and ultrapure distilled water again before drying in air at room temperature. In the next process, cyclic voltammetry analysis was separately performed for each of the catalysts. Using a syringe pump glucose and potassium hydroxide solution with concentrations of 0.1M each and glucose to KOH concentration ratio of 1:1 were flow through the sensor chamber at a flow rate of 10 μL/min. The sensor channels in each stage were rinsed using deionized water before examination as necessary. In fact it was seen that the sensor without catalyst did not have any redox peaks in the presence of glucose (Figure 27, curve 1 and curve 2) as well as potassium hydroxide solution. Whereas the ZIF8@La catalyst revealed well-defined peak in the range of 0.15-0.55 volts (Figure 27, curve 3) in the solution having glucose and potassium hydroxide the catalyst responded thus working on the substrate. In addition, the La@ZIF-8/NPC catalyst had a much larger improvement in glucose oxidation compared to the other investigated materials which could be attributed to the observed anodic peak current (Fig. 27, curve 4).

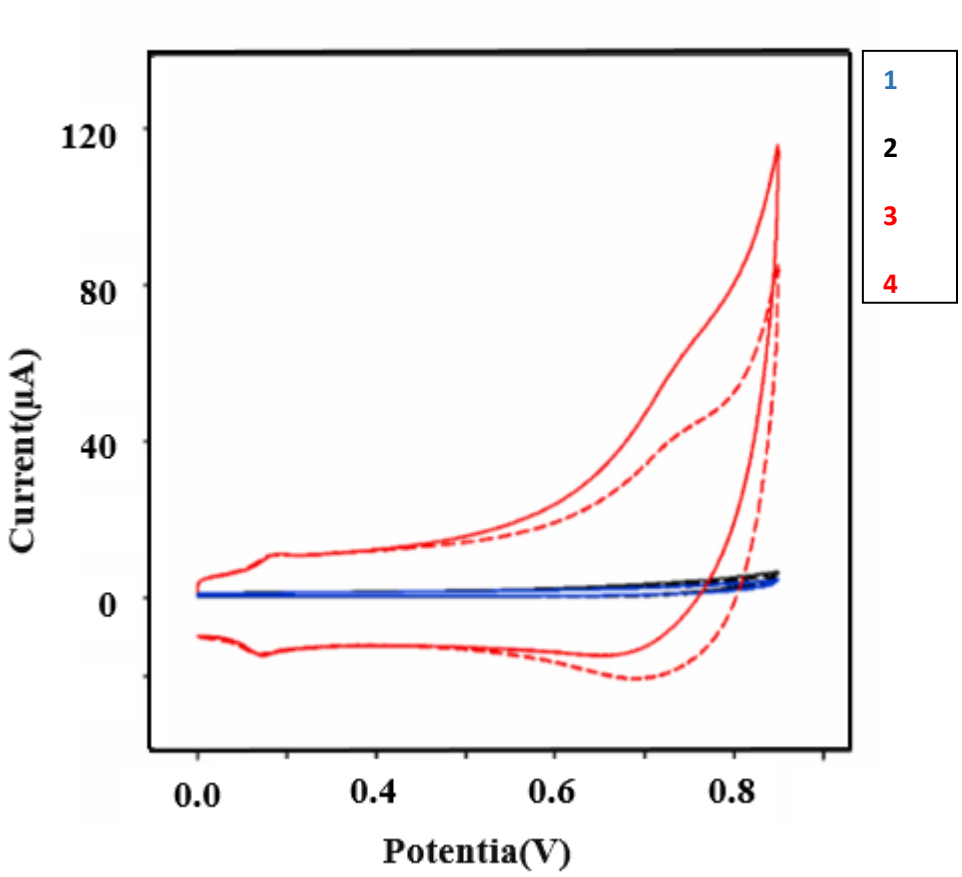

Figure 27. Redox peaks in the presence or absence of glucose: curves 1 and 2 indicate the absence of redox peaks without catalyst. Curve 3 shows the redox peak related to ZIF8/NPC. Curve 4 displays the redox peak related to La@ZIF8/NPC

6.2. Electro-catalytic study of La@ZIF-8/NPC has been conducted using both constant scan rate and concentration differences.

In the same manner as in the previous area, the electro catalytic properties of electrodes towards glucose oxidation in 0.1 M KOH solution were investigate using cyclic voltammetry. The experiment included the following glucose concentrations, 0mM, 1.5mM, 3mM, and 6mM,

Window voltage of 0-V, 0.2V, 0.4V, 0.6V and 0.8V and scan rate of 100mV/S.For this experiment, standard glucose solutions with different concentrations as well as KOH solution were prepared, while the 2 sensor input channels of the system were connected to a syringe pump. For analysis of glucose and potassium hydroxide, two solutions of each at various concentrations of 0, 25, 50 and 100 mM were pumped into the main and reference channel at a flow rate of 10 µL/minute. The glucose containing solution flowed through the main channel and above the working electrode and reference electrode at the same time; the reference channel began with the glucose solution and ended with the main channel flowing through the channel output. All the measurements were taken using Auto Lab device. The increase in glucose concentration led to a redox peak displayed in Fig. 28 attributing to the La@ZIF-8/NPC catalyst operating at the potential range of 0.55 to 0.65 V obtained enhanced balanced current response with incremental glucose concentration. It was clear that glucose oxidation took place on the surface of the La@ZIF-8/NPC/AUE. These graphs are of oxidation-reduction reactions and the players are showing oxidation by indicator losing and gaining electrons displaced by concentration of the reagent substance (glucose) and the catalyst effectively regaining its electrons. In thus cyclic process the motion starts from cathode and goes up to the peak which is the desirable process for glucose oxidation.

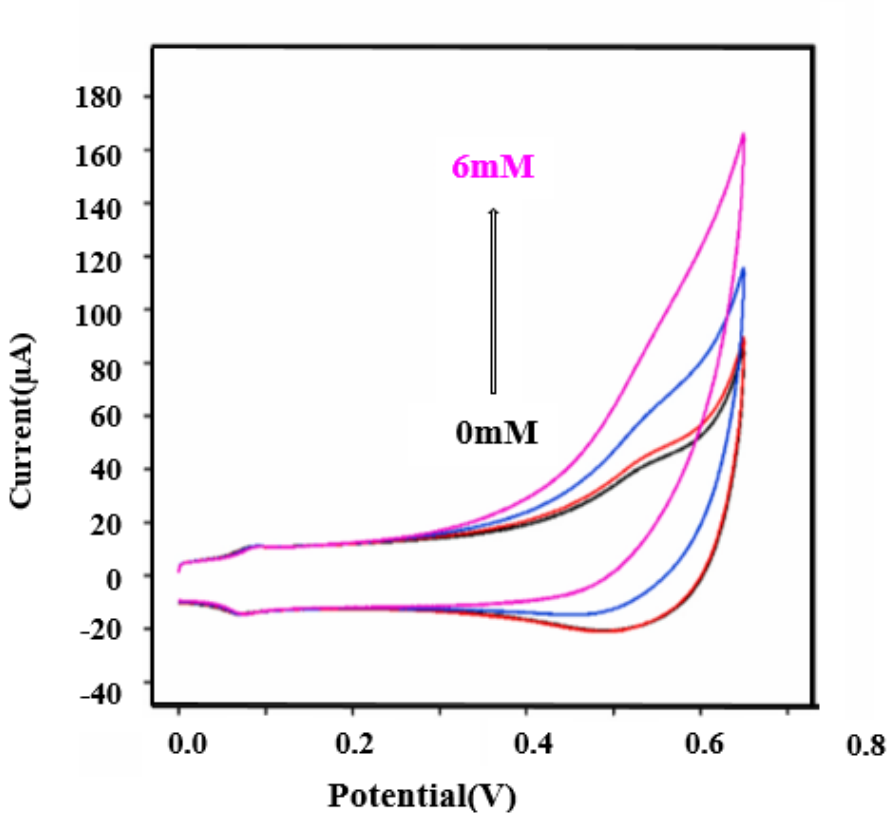

Figure 28. Cyclic voltammograms (CVs) of La@ZIF-8/NPC/AUE in 0.1 M KOH with glucose concentrations ranging from 0 to 6 mM Scan rate: 100 mV/s

6.3. Comparison Of Electrochemical Performance of La@ZIF-8/NPC Using Variable Scan Rates and Constant Concentration

The oxidation of glucose in 0.1 M KOH +0.1 M glucose was studied by cyclic voltammetry using potential range of 0-0.8V at scan rates of 20mV/s – 200mV/s. More specifically, for this experiment a solution of 0.1 M concentration of glucose and 0.1 M of K OH was prepared just like the first experiment. There were two sensor input channels connected to a syringe pump, and the solution was delivered into the main and reference channels at the rate of 10µl/min, glucose solution went into the main channel which covered both working electrode and the reference. In the case of the reference channel, the glucose solution was equilibrated by the liquid transfer in

and out, and then collected at the channel output of the main channel. All measurements were done using the Auto Lab equipment. Cyclic voltammograms were obtained in 0.1 M KOH and 0.1 M glucose solutions at different scan rates of 20-200 mV s ^{-1} within the 0-0.8 V potential range, the results of which are illustrated in Figure 29. At scan rate of 20 mV/s a small peak was noted. Thus, with the rise in scan rate, the current in both cathodic as well anodic direction which showed a controlled electrode process. The reduction of oxygen or glucose oxidation was observed in the regions of the peak between 0.45–0.65 V. The nature of this oxidation reaction appears to be diffusion-controlled since a nearly linear relationship can be obtained when graphing the square root of the scan rate versus the peak current. It is necessary therefore to incorporate figure 29 together with caption that describes the cyclic voltammograms as a function of scan rates as discussed under the figure.

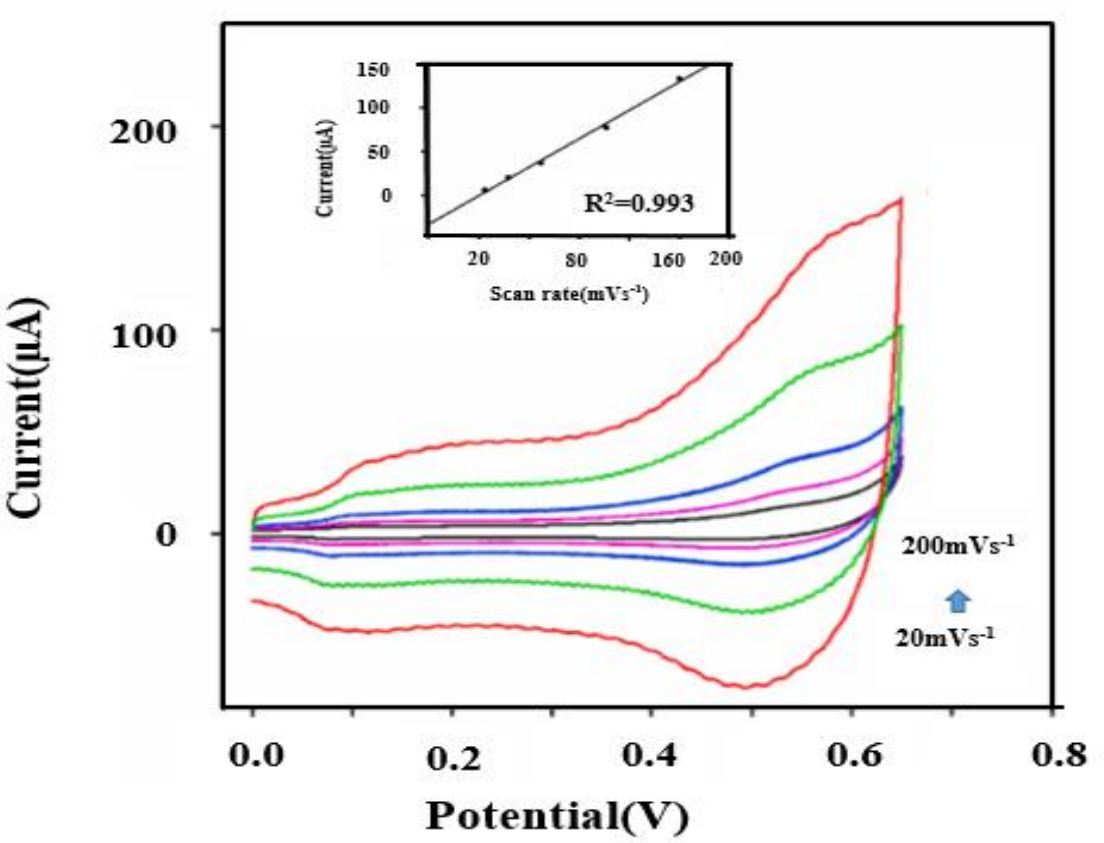

Figure 29. Cyclic voltammograms (CVs) of La@ZIF-8/NPC/AUE at scan rates ranging from 20 mV/s (black line) to 200 mV/s (red line) in 0.1 M KOH containing 0.1 M glucose. The inset plot shows the oxidation current (at 20 mV/s, vs. AU) plotted against the square root of the scan rate.

6.4. Chronoamperometry test with application of a constant potential

Chronoamperometry is an SA method where the potential is held constant at the state's value while variations in current are recorded over time. This test gives information about the substance, as far as stability and the behavior of that substance at various concentrations are concerned and is usually plotted in the form of a straight line.

6.4.1. Insights of Current Fluctuations over Time as captured by the Graph

The experiment consisted in the study of 0.1 µM glucose in a 0.1 µM potassium hydroxide solution at a constant potential of 0.55 volts; its curve was obtained. Fig 30 reveal that the

electrode process is managed and it steps into a steady or linear phase for electrode process (see figure below). With the addition of glucose concentrations, the amperometry response of La@ZIF-8/NPC/AUE was rapid, with response times of 1.3 seconds.

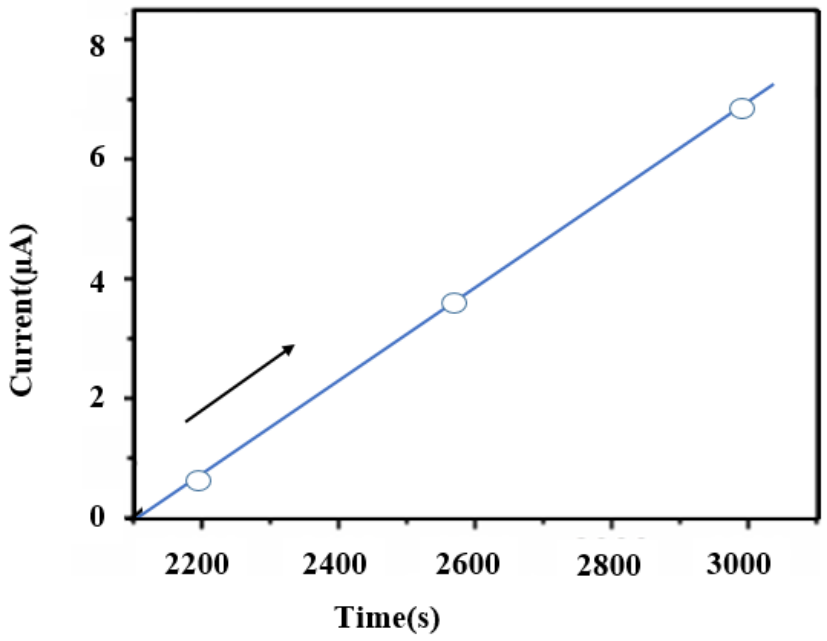

Figure 30: Linear Graph of Current Changes Over Time

6.4.2. Chronoamperometry Analysis (Analysis Based on the Current Change Graph versus Concentration Changes)

Figure 31 illustrates the ΔI values of the working electrode with varying concentrations of glucose, showing a clear increase in ΔI with increasing glucose concentration. This is followed by the peak current gradually deviating from the linear range. The calibration of variable glucose concentrations in the linear range of 0-6 μM, with a correlation coefficient of $R^2 = 0.998$, is

shown in Figure 31. A very low detection limit of 0.18 µM (S/N = 3) and a high sensitivity estimated by the slope of the line and regression equation of 35,000 µA mM^{-1} cm^{-2} were obtained. The chronoamperometry signal demonstrates a good linear relationship in the glucose concentration range from 0.8 µM to 6.0 mM

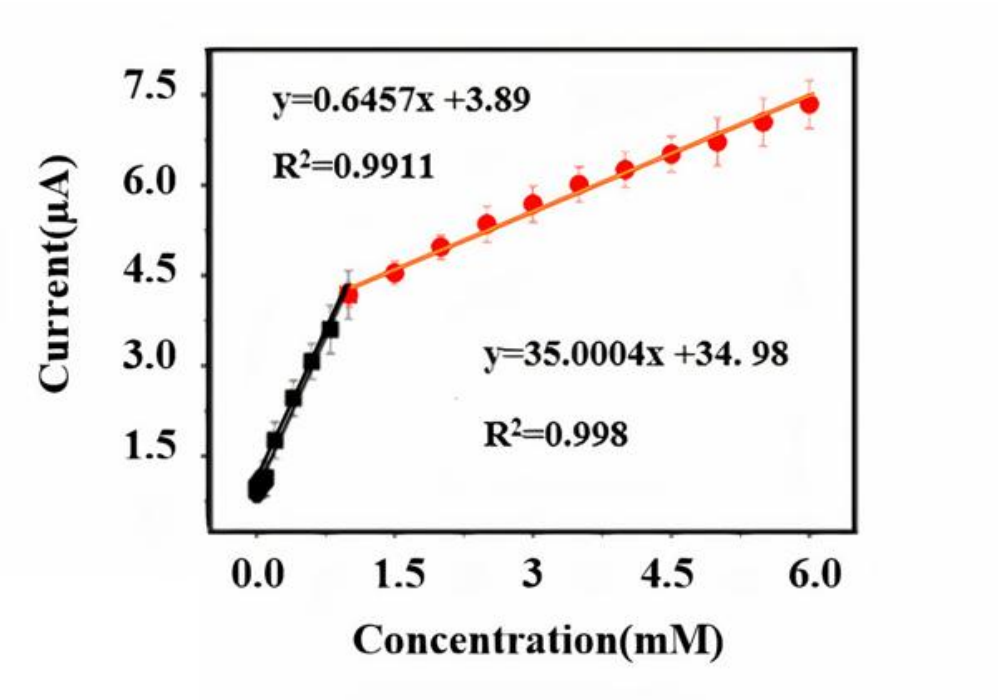

Figure 31: Linear Graph of Current Changes Based on Concentration Changes.

7.Stability and Reproducibility

The stability of the La@ZIF-8/NPC/AUE electrode was assessed through amperometry measurements, which involve measuring current over time at a fixed potential of 0.5 volts.After

prolonged continuous testing, the current recorded on the La@ZIF-8/NPC/AUE retained approximately 90% of its initial value. This indicates that even under continuous testing conditions, only a 10% decrease in current was observed, which highlights the good electrocatalytic stability of the sensor. To evaluate the sensor's long-term stability, the La@ZIF-8/NPC/AUE electrode was stored for seven days at 4 degrees Celsius and then re-tested. The current response to a concentration of 0.5 millimolar glucose still reflected 85% of its original value, demonstrating the sensor's ability to maintain stability over time. These results suggest that the sensor can deliver stable performance over extended periods and in varying conditions. The modest 10 to 15 percent decrease in current signifies that the sensor has not experienced a significant decline in electrocatalytic activity, which is generally acceptable for electrochemical sensors. To evaluate reproducibility, five independent La@ZIF-8/NPC/AUE electrodes were fabricated and tested to examine their amperometry responses to glucose. The findings revealed that these five sensors had a relative standard deviation (RSD) of less than 5 percent for their glucose responses. A low RSD indicates uniformity and consistency in the structure and performance of the sensors. The low RSD (under 5 percent) demonstrates that the fabrication and preparation process for the La@ZIF-8/NPC/AUE sensor is reliable, allowing the electrodes to produce relatively similar responses. This suggests a high level of homogeneity among the sensors and a stable manufacturing process, which are crucial for developing high-performance electrochemical sensors.

8. Accuracy

Accuracy is a function of the standard deviation. After calculating the standard deviation, we conclude that the values fall within the range of the average standard deviation. According to the

concept of accuracy, it represents the degree of closeness of measurement results to each other. Therefore, the lower the standard deviation, the more accurate the system, which holds true for this data. The accuracy value obtained is 0.009681.

A number of non-enzymatic glucose sensors based on nanoparticles have been compiled in Table 1 for comparison with La@ZIF-8/NPC/AUE. According to Table 1, it is evident that La@ZIF-8/NPC/AUE demonstrates significantly higher sensitivity, lower detection limits, and a better linear range compared to other nanoparticles. This is beneficial for advancing the development of glucose detection sensors.

La@ZIF-8/NPC exhibits greater sensitivity compared to traditional sensors. The theoretical results indicate that combining lanthanum (La) nanoparticles with ZIF-8 and petrochemical Nano carbon (NPC) provides more active sites for glucose reactions. This results in amplified electrochemical signals, leading to heightened sensitivity. The findings reveal that the La@ZIF-8/NPC composite structure offers enhanced stability over This stability arises from the prevention of structural changes and environmental interference, significantly extending the sensor's lifespan.La@ZIF-8/NPC shows strong selectivity for glucose among other sugars and substances in the environment. The theoretical results suggest that this selectivity is attributed to the presence of specific active sites and effective electrochemical measurement capabilities.

La@ZIF-8/NPC features a porous structure that aids in glucose absorption. Lanthanum (La) acts as a catalyst, while ZIF-8 serves as a carrier, facilitating easy access for glucose to the sensor's surface and enabling effective electrochemical reactions. During this process, electrons are released as glucose is oxidized, producing an electrochemical signal. Nano carbons serve as electrical conductors, enhancing the signals produced from glucose oxidation. This characteristic

helps to speed up the response time and decrease detection latency. Increased Active Surface Area The combination of different materials generates new active regions that facilitate glucose access to the sensor surface, consequently increasing the reaction rate.

Table1. Sensitivity, linear range, and detection limit of La@ZIF-8/NPC towards glucose oxidation compared with some other electrodes based on MOF nanoparticles.

Electrodes	*Sensitivity $\mu AmM^{-1}cm^{-2}$*	*Detection Limit µM*	*Reference*	*Liner range*
ZIF-8/rGO	5047.18 µA mM^{-1} cm^{-2}	0.3 µM	[32]	0.005 mM to 5 mM
ZIF-8Ni$(OH)_2$ NCs/NF	7413 µA mM^{-1} cm^{-2}	0.1 µM	[33]	1 µM to 3.45
Cu@ZIF-8(HHNs)	1594.2 µA mM^{-1} cm^{-2},	1.97 µM	[34]	5 µM to 3 mM
Ni/Cobi metal ZIF/GCE	3250 µM mM^{-1} cm^{-2}	100 nM	[35]	0.3–2.312 mM
NCNT-MOF CoCu/GCE	1027 µM $mM^{-1}cm^{-2}$	0.15 µM	[36]	0.05 to 2.5 mM
CoFe-PBA/Co-ZIF/NF	5270 µM mM^{-1} cm^{-2}	0.02 µM	[20]	1.4µM-1.5 mM
NiCo2O4 HNCs/GCE	1306 µM mM^{-1} cm^{-2}	27 nM	[37]	0.18 µM-5.1 mM
Cu-Nano spheres@ porous carbon/3D-KSC/GCE	28.67 µM mM^{-1} cm^{-2}	0.48 µM	[38]	0.15µM-5.62mM
Ag@ZIF-67/GCE	0.379 µM mM^{-1} cm^{-2}	0.66 µM	[39]	2–1000 µM
La@ZIF-8/NPC	35000 µM mM^{-1} cm^{-}	0.18 µM	---	0-6mM

9. Conclusion

The constructed La@ZIF-8/NPC/AUE was utilized as a non-enzymatic glucose sensor, with lanthanum nanoparticles successfully deposited on the AUE modified with NPC. Its advantages include very high sensitivity, excellent stability, reproducibility, low operating voltage, and a rapid amperometry response to glucose oxidation. It demonstrates a sensitivity of 35,000 μA mM^{-1} cm^{-2} at an optimal potential of 0.55 V and a correlation coefficient (R^2) of 0.998. A linear range of 0-6 mM with a low detection limit of 0.18 μM (S/N = 3) was achieved. Given the outstanding performance of La@ZIF-8/NPC/AUE, it can be considered a suitable tool for glucose determination.

CRediT authorship contribution statement

Yazdan Firouzi jahantigh: Writing – review & editing, Writing – original draft, Visualization, Validation, Methodology, Investigation, Formal analysis, Data curation. **Mehdi Mehrpooya:** Writing – review & editing, Supervision, Software, Resources, Project administration, Methodology, Investigation, Funding acquisition. **Reza Askari Moghadam:** Supervision, Methodology, Investigation, Conceptualization, Data curation, Writing – review & editing. **Mohammad Reza Ganjali:** Supervision, Methodology, Investigation, Funding acquisition, Conceptualization.

Declaration of competing interest

The authors declare that they have no known competing financial interests or personal relationships that could have appeared to influence the work reported in this paper.

Acknowledgments

The financial support of this work by the Iran National Science Foundation (INSF; Grant Number: 950019) and the University of Tehran is gratefully acknowledged.

Data availability

All data is available in the paper.

References

[1] M. Wei *et al.*, "Electrochemical non-enzymatic glucose sensors: recent progress and perspectives," *Chem. Commun.*, vol. 56, no. 93, pp. 14553–14569, 2020, doi: 10.1039/d0cc05650b.

[2] H. Abunahla *et al.*, "MOMSense: Metal-Oxide-Metal Elementary Glucose Sensor," *Sci. Rep.*, vol. 9, no. 1, 2019, doi: 10.1038/s41598-019-41892-w.

[3] S. Beg *et al.*, "Nanoporous metal organic frameworks as hybrid polymer–metal composites for drug delivery and biomedical applications," *Drug Discovery Today*, vol. 22, no. 4. 2017. doi: 10.1016/j.drudis.2016.10.001.

[4] R. Zhang, C. A. Tao, R. Chen, L. Wu, X. Zou, and J. Wang, "Ultrafast synthesis of Ni-MOF in one minute by ball milling," *Nanomaterials*, vol. 8, no. 12, 2018, doi: 10.3390/NANO8121067.

[5] S. Y. Oh *et al.*, "Skin-Attachable, Stretchable Electrochemical Sweat Sensor for Glucose and pH Detection," *ACS Appl. Mater. Interfaces*, vol. 10, no. 16, 2018, doi: 10.1021/acsami.8b03342.

[6] M. Bajgrowicz-Cieslak, Y. Alqurashi, M. I. Elshereif, A. K. Yetisen, M. U. Hassan, and H. Butt, "Optical glucose sensors based on hexagonally-packed 2.5-dimensional photonic concavities imprinted in phenylboronic acid functionalized hydrogel films," *RSC Adv.*, vol. 7, no. 85, 2017, doi: 10.1039/c7ra11184c.

[7] C. Lai *et al.*, “Metal-organic frameworks as burgeoning materials for the capture and sensing of indoor VOCs and radon gases,” *Coord. Chem. Rev.*, vol. 427, p. 213565, Jan. 2021, doi: 10.1016/J.CCR.2020.213565.

[8] M. Adeel, M. M. Rahman, I. Caligiuri, V. Canzonieri, F. Rizzolio, and S. Daniele, “Recent advances of electrochemical and optical enzyme-free glucose sensors operating at physiological conditions,” *Biosensors and Bioelectronics*, vol. 165. 2020. doi: 10.1016/j.bios.2020.112331.

[9] Y. Li *et al.*, “Co-MOF nanosheet array: A high-performance electrochemical sensor for non-enzymatic glucose detection,” *Sensors Actuators, B Chem.*, vol. 278, 2019, doi: 10.1016/j.snb.2018.09.076.

[10] Y. Ma *et al.*, “A sensitive enzyme-free electrochemical sensor based on a rod-shaped bimetallic MOF anchored on graphene oxide nanosheets for determination of glucose in huangshui,” *Anal. Methods*, vol. 15, no. 20, 2023, doi: 10.1039/d2ay01977a.

[11] H. V. Hsieh, Z. A. Pfeiffer, T. J. Amiss, D. B. Sherman, and J. B. Pitner, “Direct detection of glucose by surface plasmon resonance with bacterial glucose/galactose-binding protein,” *Biosens. Bioelectron.*, vol. 19, no. 7, pp. 653–660, 2004, doi: 10.1016/S0956-5663(03)00271-9.

[12] V. Scognamiglio, “Nanotechnology in glucose monitoring: Advances and challenges in the last 10 years,” *Biosensors and Bioelectronics*, vol. 47. pp. 12–25, Sep. 05, 2013. doi: 10.1016/j.bios.2013.02.043.

[13] N. Papageorgiou, “Machine-learning helps sort out massive MOF materials’ databases,” *Nanowerk*, 2020, Accessed: May 05, 2024. [Online]. Available: https://www.nanowerk.com/nanotechnology-news2/newsid=56159.php

[14] A. E. G. Cass *et al.*, “Ferrocene-Mediated Enzyme Electrode for Amperometric Determination of Glucose,” *Anal. Chem.*, vol. 56, no. 4, pp. 667–671, 1984, doi: 10.1021/ac00268a018.

[15] X. Zhang *et al.*, "MOF-derived Porous NiO Nanorod and Microflower Structures with Enhanced Non-enzymatic Glucose Electrochemical Sensing Performance," *Int. J. Electrochem. Sci.*, vol. 16, pp. 1–11, 2021, doi: 10.20964/2021.04.65.

[16] S. Xi *et al.*, "Integration of carbon nanotubes to three-dimensional C-MEMS for glucose sensors," *Sensors Actuators, A Phys.*, vol. 198, pp. 15–20, 2013, doi: 10.1016/j.sna.2013.04.004.

[17] C. W. Bae *et al.*, "Fully Stretchable Capillary Microfluidics-Integrated Nanoporous Gold Electrochemical Sensor for Wearable Continuous Glucose Monitoring," *ACS Appl. Mater. Interfaces*, vol. 11, no. 16, 2019, doi: 10.1021/acsami.9b00848.

[18] M. Govindaraj *et al.*, "Current advancements and prospects of enzymatic and non-enzymatic electrochemical glucose sensors," *Int. J. Biol. Macromol.*, vol. 253, 2023, doi: 10.1016/j.ijbiomac.2023.126680.

[19] P. U. Abel and T. Von Woedtke, "Biosensors for in vivo glucose measurement: Can we cross the experimental stage," *Biosens. Bioelectron.*, vol. 17, no. 11–12, 2002, doi: 10.1016/S0956-5663(02)00099-4.

[20] C. Chen, D. Xiong, M. Gu, C. Lu, F. Y. Yi, and X. Ma, "MOF-Derived Bimetallic CoFe-PBA Composites as Highly Selective and Sensitive Electrochemical Sensors for Hydrogen Peroxide and Nonenzymatic Glucose in Human Serum," *ACS Appl. Mater. Interfaces*, vol. 12, no. 31, pp. 35365–35374, 2020, doi: 10.1021/acsami.0c09689.

[21] P. H. Huang *et al.*, "Ag@Au nanoprism-metal organic framework-based paper for extending the glucose sensing range in human serum and urine," *Dalt. Trans.*, vol. 46, no. 21, pp. 6985–6993, 2017, doi: 10.1039/c7dt00875a.

[22] T. Raj kumar, G. Gnana kumar, and A. Manthiram, "Biomass-Derived 3D Carbon Aerogel with Carbon Shell-Confined Binary Metallic Nanoparticles in CNTs as an Efficient Electrocatalyst for

Microfluidic Direct Ethylene Glycol Fuel Cells," *Adv. Energy Mater.*, vol. 9, no. 16, 2019, doi: 10.1002/aenm.201803238.

[23] M. Pappathi *et al.*, "Trimetallic ZIF-Derived Ni-Cu/NC Rhombic Dodecahedron Nanostructures on Butter Sheet Paper as a Flexible Electrochemical Probe for Nonenzymatic Glucose Sensors," *ACS Appl. Nano Mater.*, vol. 6, no. 16, 2023, doi: 10.1021/acsanm.3c01489.

[24] M. Hilal, W. Xie, and W. Yang, "Straw-sheaf–like Co3O4 for preparation of an electrochemical non-enzymatic glucose sensor," *Microchim. Acta*, vol. 189, no. 9, pp. 1–11, Sep. 2022, doi: 10.1007/S00604-022-05453-9/METRICS.

[25] G. Gnana Kumar, S. H. Chung, T. Raj Kumar, and A. Manthiram, "Three-Dimensional Graphene-Carbon Nanotube-Ni Hierarchical Architecture as a Polysulfide Trap for Lithium-Sulfur Batteries," *ACS Appl. Mater. Interfaces*, vol. 10, no. 24, 2018, doi: 10.1021/acsami.8b06054.

[26] K. Ramachandran, T. Raj Kumar, K. J. Babu, and G. Gnana Kumar, "Ni-Co bimetal nanowires filled multiwalled carbon nanotubes for the highly sensitive and selective non-enzymatic glucose sensor applications," *Sci. Rep.*, vol. 6, 2016, doi: 10.1038/srep36583.

[27] Z. Ren *et al.*, "A Non-enzymatic Glucose Sensor Based on Graphene Modified Copper-Nickel Bimetallic Dendrite Structure," *ChemistrySelect*, vol. 7, no. 41, 2022, doi: 10.1002/slct.202202522.

[28] G. Siva, M. A. Aziz, and G. Gnana Kumar, "Engineered Tubular Nanocomposite Electrocatalysts Based on CuS for High-Performance, Durable Glucose Fuel Cells and Their Stack," *ACS Sustain. Chem. Eng.*, vol. 6, no. 5, 2018, doi: 10.1021/acssuschemeng.7b04326.

[29] K. Omri and N. Alonizan, "Enhanced photocatalytic performance and impact of annealing temperature on TiO2/Gd2O3:Fe composite," *J. Mater. Sci. Mater. Electron.*, vol. 33, no. 19, pp. 15448–15459, Jul. 2022, doi: 10.1007/S10854-022-08451-Y/METRICS.

[30] K. Omri, I. Najeh, S. Mnefgui, N. Alonizan, and S. Gouadria, "Microstructure, AC conductivity and

complex modulus analysis of Ca-ZnO nanoparticles for potential optoelectronic applications," *Mater. Sci. Eng. B*, vol. 297, p. 116738, Nov. 2023, doi: 10.1016/J.MSEB.2023.116738.

[31] K. Omri, N. Alonizan, R. A. Abumousa, M. Alqahtani, and T. Ghrib, "Fabrication and enhanced UV-light photocatalytic performance of Mn2O3/Dy2O3 nanocomposites," *J. Mater. Sci. Mater. Electron.*, vol. 34, no. 5, pp. 1–12, Feb. 2023, doi: 10.1007/S10854-023-09875-W/METRICS.

[32] K. Kim, S. Kim, H. N. Lee, Y. M. Park, Y. S. Bae, and H. J. Kim, "Electrochemically derived CuO nanorod from copper-based metal-organic framework for non-enzymatic detection of glucose," *Appl. Surf. Sci.*, vol. 479, pp. 720–726, 2019, doi: 10.1016/j.apsusc.2019.02.130.

[33] F. Xu *et al.*, "ZIF-8 derived Ni(OH)2 hollow nanocages for non-enzymatic glucose electrochemical sensing," *J. Mater. Sci.*, vol. 57, no. 39, pp. 18589–18600, Oct. 2022, doi: 10.1007/S10853-022-07771-Y.

[34] Q. Zhu *et al.*, "Reconstructing hydrophobic ZIF-8 crystal into hydrophilic hierarchically-porous nanoflowers as catalyst carrier for nonenzymatic glucose sensing," *Sensors Actuators B Chem.*, vol. 313, p. 128031, Jun. 2020, doi: 10.1016/J.SNB.2020.128031.

[35] Z. Xu, Q. Wang, H. Zhangsun, S. Zhao, Y. Zhao, and L. Wang, "Carbon cloth-supported nanorod-like conductive Ni/Co bimetal MOF: A stable and high-performance enzyme-free electrochemical sensor for determination of glucose in serum and beverage," *Food Chem.*, vol. 349, 2021, doi: 10.1016/j.foodchem.2021.129202.

[36] S. eun Kim and A. Muthurasu, "Highly Oriented Nitrogen-doped Carbon Nanotube Integrated Bimetallic Cobalt Copper Organic Framework for Non-enzymatic Electrochemical Glucose and Hydrogen Peroxide Sensor," *Electroanalysis*, vol. 33, no. 5, pp. 1333–1345, 2021, doi: 10.1002/elan.202060566.

[37] Y. Feng *et al.*, "MOF-Derived Spinel NiCo2O4 Hollow Nanocages for the Construction of Non-

enzymatic Electrochemical Glucose Sensor," *Electroanalysis*, vol. 32, no. 3, pp. 571–580, 2020, doi: 10.1002/elan.201900558.

[38] Y. Xie *et al.*, "Cu metal-organic framework-derived Cu Nanospheres@Porous carbon/macroporous carbon for electrochemical sensing glucose," *J. Alloys Compd.*, vol. 757, pp. 105–111, 2018, doi: 10.1016/j.jallcom.2018.05.064.

[39] W. Meng, Y. Wen, L. Dai, Z. He, and L. Wang, "A novel electrochemical sensor for glucose detection based on Ag@ZIF-67 nanocomposite," *Sensors Actuators, B Chem.*, vol. 260, 2018, doi: 10.1016/j.snb.2018.01.109.